HIV-1 Nef Hijacks Lck and Rac1 Endosomal Traffic To Dually Modulate Signaling-Mediated and Actin Cytoskeleton–Mediated T Cell Functions

Iratxe del Río-Iñiguez, Elena Vázquez-Chávez, Céline Cuche, Vincenzo Di Bartolo, Jérôme Bouchet, Andres Alcover

Accepted manuscript without last corrections:

Reference of the article published

Del Río-Iñiguez, I., Vázquez-Chávez, E., Cuche, C., Di Bartolo, V., Bouchet, J. and Alcover, A. 2018. HIV-1 Nef Hijacks Lck and Rac1 Endosomal Traffic To Dually Modulate Signaling-Mediated and Actin Cytoskeleton-Mediated T Cell Functions. Journal of Immunology, 201(9):2624-2640. doi: 10.4049/jimmunol.1800372.

HIV-1 Nef hijacks Lck and Rac1 endosomal traffic to dually modulate signaling- and actin cytoskeleton-mediated T cell functions.

Iratxe del Río-Iñiguez[*,†,§], Elena Vázquez-Chávez[*,†], Céline Cuche[*,†], Vincenzo Di Bartolo[*,†], Jérôme Bouchet[*,†,1,2] and Andrés Alcover[*,†,2]

[*]Institut Pasteur, Department of Immunology, Lymphocyte Cell Biology Unit, Paris. France.
[†]INSERM U1221. Paris France.
[§]Sorbonne Université, Collège Doctoral, Paris, France

Running title: Nef hijacks T cell signaling and cytoskeletal regulators

Correspondence:

Andrés Alcover PhD. Institut Pasteur, Unité de Biologie Cellulaire des Lymphocytes. 28, Rue Dr Roux. 75724 Paris Cedex 15. France. Tel: office +33 1 40 61 30 64 // cellular: +33 6 84 47 22 30. Email: andres.alcover@pasteur.fr

Jérôme Bouchet, PhD. Institut Cochin INSERM, U1016, CNRS, UMR8104, Université Paris Descartes, Sorbonne Paris Cité, Paris, France. Email: jerome.bouchet@inserm.fr

Abstract

Endosomal traffic of TCR and signaling molecules regulates immunological synapse formation and T cell activation. We recently showed that Rab11 endosomes regulate the subcellular localization of the tyrosine kinase Lck and of the GTPase Rac1 and control their functions in TCR signaling and actin cytoskeleton remodeling. HIV-1 infection of T cells alters their endosomal traffic, activation capacity and actin cytoskeleton organization. The viral protein Nef is pivotal for these modifications. We hypothesized that HIV-1 Nef could jointly alter Lck and Rac1 endosomal traffic and concomitantly modulate their functions. Here, we show that HIV-1 infection of human T cells sequesters both Lck and Rac1 in a pericentrosomal compartment in a Nef-dependent manner. Strikingly, the Nef-induced Lck compartment contains signaling competent forms (phosphorylated on key Tyr residues) of Lck and some of its downstream effectors, TCRζ, ZAP70, SLP76 and Vav1, avoiding the proximal LAT adaptor. Importantly, Nef-induced concentration of signaling molecules was concomitant with the upregulation of several early and late T cell activation genes. Moreover, preventing the concentration of the Nef-induced Lck compartment, by depleting the Rab11 effector FIP3, counteracted Nef-induced gene expression upregulation. In addition, Nef extensively sequesters Rac1 and down regulates Rac1-dependent actin cytoskeleton remodeling, thus reducing T cell spreading. Therefore, by modifying their endosomal traffic, Nef hijacks signaling and actin cytoskeleton regulators to dually modulate their functional outputs. Our data shed new light into the molecular mechanisms that modify T cell physiology during HIV-1 infection.

Introduction

Antigen recognition triggers T cell polarization towards the antigen presenting cell (APC). This process involves the reorganization of the actin and microtubule cytoskeleton, the reorientation of intracellular vesicle traffic and the generation of dynamic signaling and adhesion complexes at the T cell-APC contact site, termed the immunological synapse. Altogether, these processes control immunological synapse formation and function, ensuring T cell activation leading to T cell proliferation and differentiation, and T cell effector functions, like polarized secretion of cytokines and cytotoxic granules (1, 2).

TCR signal transduction involves the CD3γ, δ, ε and ζ subunits, which contain in their intracellular regions immune-receptor tyrosine-based activation motifs (ITAM) that are phosphorylated soon after TCR engagement. ITAM phosphorylation by the Src family protein tyrosine kinase Lck facilitates the recruitment of downstream effectors, including the tyrosine kinase ZAP70 (zeta-associated protein of 70 kDa), which is recruited to phosphorylated ITAMs of TCRζ *via* its SH2 domains. This induces ZAP70 tyrosine phosphorylation and activation, the subsequent tyrosine phosphorylation of the signaling adaptors LAT and SLP76 and the recruitment of effectors to these adaptors. Altogether, these proteins form a signalosome necessary to proceed to downstream activation events, including the activation of phospholipase C (PLC)-γ1, the generation of lipid second messengers, calcium flux, and the activation of serine-threonine kinases, like MAP and protein kinase C (PKC) kinases. The coordinated action of these different signaling molecules drives the activation of transcription factors (e. g. NFAT, NFκB and AP1), which in turn activate the expression of genes involved in T cell growth, differentiation and the production of cytokines, crucial for the development of adaptive immune responses (3, 4).

HIV-1 infects $CD4^+$ T cells, subverting a variety of T cell physiological mechanisms. This facilitates the production of viral particles and their transmission to other cells eventually leading to chronic viral infection, while reducing the impact of the host immune defenses. HIV-1 genome encodes several "accessory" proteins that are key for the HIV-1 subversion of infected cell processes. Among them, Nef is crucial for *in vivo* viral replication, and AIDS pathogenesis. Nef is abundantly expressed early after infection and optimizes the intracellular environment to improve virus replication and reduce host immunity by modulating endosomal traffic, actin cytoskeleton components and cell activation in infected T cells. As a consequence, HIV-1 infection modifies the expression of several T cell surface molecules, including CD4, CD28, MHC I and II (5), it alters cytoskeleton remodeling and its associated

cellular events (6-14), and it modulates T cell activation by affecting various signaling pathways (15, 16). HIV-1 Nef interferes with Lck and LAT endosomal traffic to the immunological synapse, altering T cell activation (17-19). The action of Nef on these processes occurs through the presence of specific motifs in its primary sequence, allowing interactions with a number of cellular proteins. Nef may also modify some intracellular traffic pathways, resulting in the modulation of processes regulated by proteins transported through those pathways.

We and others have shown that the TCR and the signaling molecules Lck and LAT are associated with distinct endosomal and Golgi intracellular compartments. Their traffic to the immunological synapse is differentially regulated and is crucial for TCR signal transduction (20-30). Interestingly, we also observed that the GTPase Rac1, a key actin cytoskeleton regulator, is also associated with recycling endosomes that control Rac1 subcellular localization, its targeting to the immunological synapse and its ability to regulate actin remodeling in T cells (31, 32).

Here, we performed a systematic analysis of the potential interplay between HIV-1 Nef and the T cell activation molecular machinery, by analyzing its capacity to control the subcellular localization and activation of signaling molecules downstream of the TCR, and its consequence for T cell physiology. Our results show that Nef exerts a refined control of signaling and cytoskeleton regulators to modulate T cell activation and cytoskeleton mediated events.

Materials and Methods

Expression vectors, small interfering RNA, viruses, primers and antibodies

Vectors encoding green fluorescent protein (GFP), WT and mutant GFP-tagged HIV-1 NL4-3 Nef (Nef-GFP and Nef PXXP/AXXA-GFP) were previously described (33, 34). Wild type and Nef-deleted (NL4-3-based) proviral plasmids (HIV-1 WT and HIV-1 ΔNef, respectively) have already been described (35, 36). pCMV-VSV-G was a gift from R. Weinberg (Addgene plasmid # 8454) (37).

FIP3 was depleted with siRNA duplexes based on human FIP3 sequence described elsewhere: siFIP3.1 (5'-AAGGGATCACAGCCATCAGAA-3') and siFIP3.2 (5'-AAGGCAGTGAGGCGGAGCTGTT-3') (28, 31).

Virions were produced by the transient calcium-phosphate DNA precipitation technique. HEK293T cells were transfected with 20 µg proviral DNA. 72 h later supernatant was recovered, centrifuged and cell free virion stocks were stored at -80°C. The concentration of p24 antigen in viral stocks was measured by a quantitative enzyme-linked immunosorbent assay (Perkin Elmer).

Antibodies and primer sequences are described in detail in the Supplemental Tables 1-3.

Cells, cell culture, infection and transfection assays

Human peripheral blood T cells from healthy volunteers were obtained from the French National Blood Bank (Etablissement Français du Sang, EFS) and through the ICAReB core facility at the Institut Pasteur (NSF96-900 certified, from sampling to distribution, reference BB-0033-00062/ICAReB platform/ Institut Pasteur, Paris, France/BBMRI AO203/ 1 distribution/access: 2016, May 19th, [BIORESOURCE]), under the CoSImmGEn protocol approved by the Committee of Protection of Persons, Ile de France-1 (no. 2010-dec-12483). Informed consent was obtained from all subjects. Peripheral blood mononuclear cells (PBMCs) were isolated by centrifugation through Ficoll-Hypaque from healthy donors. PBMCs were cultured in RPMI 1640 medium containing 10% foetal calf serum (FCS), 1 mM sodium pyruvate and 1% Penicillin-Streptomycin. For HIV-1 infection assays, PBMCs were cultured with 5 µg/mL PHA for two days, then infected with the equivalent of 2 µg/mL of capside protein of 24 kDa (p24) of either WT or ΔNef HIV-1 virions during 16 h. Cells were then washed and resuspended in RPMI 1640 medium supplemented with 10% FCS and 10U/mL IL-2 for 3 days, before been used for immunofluorescence assays.

For transfection assays of primary cells, $CD4^+$ T cells were further purified using the $CD4^+$ T cell isolation kit (Miltenyi Biotech) and cultured in RPMI 1640 medium containing

10% FCS, 1 mM sodium pyruvate, and nonessential amino acids. Isolated $CD4^+$ T cells were transfected with 10 µg plasmid DNA using the Amaxa Nucleofector system and the Human T Cell Nucleofector kit (Lonza). Cells were harvested and used for immunofluorescence analysis 24 h after transfection.

The human T cell line Jurkat clone J77cl20 was previously described (17). Jurkat were cultured in RPMI 1640 containing 10% FCS. For HIV-1 infection assays, $5x10^6$ Jurkat cells were infected with 2 µg of cell free HIV-1 virions or VSV-pseudotyped virions during 16 h. Cells are then washed and resuspended in RPMI 1640 medium supplemented with 10% FCS for 3 days (or 36 h for the VSV-pseudotyped virions), before being harvested.

For siRNA, a total of 2 nmol of control or FIP3 siRNA were used per 10^7 Jurkat cells. 2 transfections were performed at 24 h interval with a Neon Transfection system (Life Technologies), using the following protocol: 1400 V, 10 ms, 3 pulses. 72 h after the first transfection cells were harvested and processed for analysis. In the case of plasmid transfection, the Neon Transfection system was used in the same conditions to electroporate 10^7 Jurkat cells with 10 µg plasmid DNA. Cells were harvested and processed for analysis 24 h after the transfection. When both infection and FIP3 depletion conditions were applied, Jurkat cells were previously transfected with siRNA, and consecutively infected with VSV-pseudotyped virions for 36 h, with a total of 72 h from the first transfection, before the cells were harvested and processed for analysis.

Immunofluorescence

Immunofluorescence and confocal imaging was performed as previously described (38, 39). Coverslips were coated with poly-L-lysine 0.002 % (w/v) in water (Sigma-Aldrich). Cells were plated onto the coverslips for 3 min (if not otherwise indicated), then fixed with 4 % paraformaldehyde for 20 min at room temperature (RT), washed in phosphate buffer saline (PBS), and incubated 30 min in PBS, 1 % bovine serum albumin (wt/vol) (PBS-BSA) to prevent unspecific binding. Coverslips were then incubated 1 h at RT in PBS-BSA with 0.1 % Triton X-100 and the indicated dilution of primary antibody. Coverslips were rinsed 3 times in PBS-BSA and then incubated with the corresponding fluorescent-coupled secondary antibody for 1 h at RT. After 3 washes in PBS-BSA, coverslips were mounted on microscope slides using 8 µl of ProLongGold Antifade mounting medium with DAPI (Life Technologies).

Confocal microscopy, image post-treatment and analysis

Confocal images were acquired with a LSM 700 confocal microscope (Carl Zeiss) using the Plan-Apochromat 63x objective. Optical confocal sections were acquired using ZEN software (Carl Zeiss) by intercalating green and red laser excitation to minimize channel cross talk. Confocal optical sections were acquired at 0.2 μm depth intervals and images were treated by deconvolution with the Huygens Pro Software (version 14.10, Scientific Volume Imaging). A 2D visualization of 3 consecutive confocal sections (cut of 0.4 μm depth,) centered on the Nef induced endosomal compartment, when visible, or on a mid-section of the cell, was generated from a sum intensity projection using Fiji software (40). Images showing the density gradient fluorescent intensities were obtained with the mpl-Inferno LUT of Fiji software.

Colocalization analyses were performed on the whole compartment (Nef, Lck or Rac1) of deconvoluted images using Fiji software and the JACoP plugin (41). Threshold was automatically determined using the Costes method autothreshold determination (42). Analysis plots show the Pearson Correlation Coefficient. Colocalization scatter plot images show one representative colocalization analysis of the whole analysis and were obtained using the Colocalization Threshold plugin of the Fiji software. Statistical analyses were carried out using the nonparametrical Mann-Whitney test of Prism software (Graphpad).

Images to quantify phospho-protein accumulation in the Lck compartment were acquired at 1μm depth intervals in the z-axis to avoid fluorescence overlap. Fluorescence intensity in the area corresponding to the Lck compartment was calculated in percentage of the total fluorescence of the cell. Statistical analyses were carried out using the nonparametrical Mann-Whitney test of Prism software (Graphpad).

For densitometry profile analysis, a z-stack of 1 μm confocal optical sections was acquired for each cell. Fluorescence intensity of pY319-ZAP70 or Rac1 was measured across cells, including plasma membrane and the Nef pericentrosomal compartment.

Analysis of cell spreading

Cells were plated on poly-L-lysine coated coverslips, incubated at RT for the indicated times and fixed with 4 % paraformaldehyde for 20 min. Coverslips were then treated as previously described in the immunofluorescence section above, using a phalloidin labeled antibody to stain F-actin. For the measurement of cell spreading, z-stacks of 0.5 μm confocal optical sections were acquired. Two contiguous sections starting from the coverslip surface were stacked, and cell surface was measured on the phalloidin staining using the Fiji Analyse

Particles tool, on GFP positive particles larger than 20 μm^2. Statistical analyses were carried out using the nonparametrical Mann-Whitney test of Prism software (Graphpad).

Activation analysis

Cells were stimulated by incubation with 10 μg/mL of soluble CD3 mouse antibody (UCHT1) and 10 μg/mL of CD28 at 37°C. At the indicated times, cells were plated on poly-L-lysine coated coverslips as previously described, fixed with 4 % paraformaldehyde for 20 min at RT, washed in PBS and incubated 30 min in PBS-BSA before immunofluorescence was performed.

Flow cytometry

Infection levels were analyzed by flow cytometry using a MACSQuant Analyzer (Miltenyi biotech). Cells were isolated, fixed with 4 % paraformaldehyde for 20 min at RT, washed in PBS, and incubated with the appropriate dilution of fluorescent-labeled antibody in PBS-BSA. For fluorescence intensity levels of intracellular phospho-proteins, fixed cells were incubated in PBS-BSA with 0.1 % Triton X-100 and the indicated dilution of primary antibody and secondary fluorescent-labeled antibody. Flow cytometry data were analyzed with FlowJo software (FlowJo, LLC), restricting the analyses to single-cells using FSC-H/W signals.

Western blot

Cells were lysed for 30 min in ice-cold buffer composed of 150 mM NaCl, 20 mM Tris pH 7.4, 0.25 % lauryl-β-maltoside, 4 mM orthovanadate, 1 mM EGTA, 50 mM NaF, 10 mM $Na_4P_2O_7$, 1mM $MgCl_2$ and protease inhibitors (1mM AEBSF, 10 μg/mL Aprotinin, 10 μg/mL Leupeptin). Cells lysates were centrifuged at 20,800 xg for 10 min at 4°C. Equal amount of protein extract was loaded in NuPAGE 4-12% Bis-Tris gels (Life Technologies) by using the BCA assay Kit (Thermo Fisher Scientific). Protein transfer to nitrocellulose blots (LI-COR Biosciences) was performed using the BIO-RAD system and a transfer buffer composed of 25 mM Tris, 1,92 mM Glycine, 20 % EtOH, 0.1 % SDS. Membranes were saturated with blocking buffer (Rockland Immunochemicals) and incubated with primary antibodies for 1 h at RT or overnight at 4°C in blocking buffer. After incubation with secondary antibodies, an Odyssey scanner (LI-COR Biosciences) was used to detect and imaged near-infrared fluorescence. Images of blots were quantified using Fiji software.

mRNA measurements by RT-qPCR

Total RNA was extracted using the RNeasy Mini Plus Kit (Qiagen), following the manufacturer's instructions. cDNA was prepared from 1 μg of total RNA using iScript cDNA synthesis kit (BIO-RAD). Gene products were quantified by qPCR using the FastStart Universal SYBR Green PCR master mix (Roche) and the ABI PRISM 7900HT technology. Most of the cases, qPCR quantifications were performed at least in 3 replicates and its quantity values were calculated by the Relative Standard Curve Method and normalized to the mRNA expression of the *B2M* housekeeping gene.

Primer sequences used to target the different genes are described in Supplemental Table-3.

Statistics

Statistical analyses were carried out using Prism software (Graphpad V.7). Details about the data presentation, the experimental replication, and the adequate statistical tests used are included in the individual Fig. legends. Data met the assumptions of the statistical tests and its distribution was previously checked using the Shapiro-Wilk normality test. Horizontal bars in plots represent the mean ± SEM. p values are represented as follow: ****, $p<0.0001$; ***, $p<0.001$; **, $p<0.01$; *, $p<0.05$; non-significant (ns), $p \geq 0.05$.

Results

HIV-1 sequesters Lck and Rac1 in intracellular compartments in a Nef-dependent manner.

We and others have shown that HIV-1 Nef subverts the intracellular traffic of Lck and its function as a TCR signaling molecule at the immunological synapse (17-19, 43). The molecular mechanism involved in Lck retention by Nef is not completely elucidated, and may involve, at least in part, the Lck traffic regulatory protein Unc119 and the transferrin recycling endosomal compartment (17, 19, 34) that are regulated by the Rab11 GTPase (22, 44).

We have recently shown that Lck is associated with the $Rab11^+$ endosomal compartment and its function in TCR signaling is regulated by the Rab11 effector FIP3 (Rab11 family interacting protein-3) (28). Interestingly, T cells overexpressing FIP3 retain Lck in their $Rab11^+$ endosomal compartment, in a similar manner than Nef (17, 28). Moreover, we have shown that Rac1 is also associated with $Rab11^+$ endosomes and its

subcellular localization and function are regulated by FIP3 (31). These findings prompted us to hypothesize that Nef could jointly alter Lck and Rac1 endosomal traffic, modulating their functions concomitantly. Therefore, we analyzed the intracellular localization of Lck and Rac1 upon HIV-1 infection by wild type (WT) and Nef-deficient (ΔNef) viruses, as well as in T cells expressing a Nef-GFP chimeric protein.

We indeed observed that HIV-1 infection in both primary and Jurkat T cells induced the accumulation of Lck and Rac1, in a Nef-dependent manner. Lck and Rac1 concentrate in the pericentrosomal area, while partially disappear from their cortical localization (Fig. 1A-1D). Moreover, expression of Nef alone was sufficient for the intracellular relocalization of both Lck and Rac1(Fig. 2A, 2C). Both molecules colocalized with Nef, although the overlap of Rac1 and Nef was more extensive than that of Nef and Lck (Fig. 2A-2C, 8A). The Nef-induced Lck compartment colocalized with Rab11 and not with TGN46, indicating that Lck is mainly located in recycling endosomes (Fig. 2D, 2E).

Hence, HIV-1 Nef is necessary and sufficient to induce the concomitant intracellular relocalization of Lck and Rac1 in intracellular compartments, prompting us to investigate the characteristics and functional consequences of these compartments.

Nef-induced Lck endosomal compartment concentrates active Lck together with signaling competent TCRζ, ZAP70, SLP76 and Vav1.

Lck kinase activity is regulated by the balanced phosphorylation of two tyrosine residues, Tyr394, which favors kinase activity and substrate interaction, and Tyr505, which prevents it, by stabilizing Lck in a folded conformation. The two species are present at equilibrium in resting T cells and their phosphorylation ratio does not change upon TCR engagement (45). This suggests that TCR signal transduction may be triggered by changes in localization of active forms of Lck that facilitate Lck contiguity to its substrates (e. g. delivery of endosomes carrying Lck to the immunological synapse). In this line, we have recently shown that modifying the endosomal localization of Lck changes the activation capacity of T cells, as assessed by the phosphorylation status of Lck and ZAP70 substrates (28).

To investigate the potential functional effects of Nef-induced endosomal accumulation of Lck, we analyzed whether active forms of Lck were present in that compartment and if so, whether there was an effect on Lck substrates and downstream effectors. To this end, we performed a systematic analysis in Jurkat T cells expressing GFP-tagged Nef protein. This

experimental set up provides sufficient spatial resolution to analyze these vesicular compartments, while eliminating the influence of other viral proteins. The use of specific antibodies directed to phosphorylated tyrosine (pTyr) residues allowed us to distinguish whether signaling molecules were in their signaling-competent phosphorylated state (e.g. pTyr residues described to interact with other signaling molecules).

We observed that active phosphorylated Lck (pTyr394) concentrates in the Nef-induced Lck compartment (Fig. 2B). Moreover, the phosphorylated forms of TCRζ (pTyr142) and ZAP70 (pTyr319), both substrates of Lck and interacting with each other upon TCRζ phosphorylation, are enriched within the Lck endosomal compartment, in which significantly colocalize with Lck (Fig. 3A, 3B, 4A). Interestingly, the signaling adaptors LAT and SLP76 that interact which each other upon LAT phosphorylation by ZAP70 (3), are differentially concentrated at the Nef-induced Lck compartment: pLAT (pTyr191) is neither concentrated nor colocalized with Lck, while pSLP76 (pTyr128) accumulates and colocalizes with Lck, but to a lesser extent than pTCRζ and pZAP70 (Fig. 3C, 3D, 4A). Therefore, these findings show that Nef sequesters the "initial triggering complex" formed by Lck, TCRζ and ZAP70, apparently separating the two components of the "signal amplification complex" formed by the phosphorylated adaptors LAT and SLP76 (3, 4).

Importantly, concentration of phosphorylated Lck substrates in the pericentrosomal compartment was related with Lck accumulation, since overexpression of the Nef $P_{72}XXP_{75}$/AXXA mutant, which does not induce Lck accumulation (46), does not result in pZAP70 accumulation (Fig. 4B, 4C). Moreover, the capacity of Nef to increase total pZAP70, as assessed by flow cytometry, was significantly reduced in cells expressing the Nef $P_{72}XXP_{75}$/AXXA mutant (Fig. 4D).

In addition, we found phosphorylated Vav1 (pTyr174) significantly concentrated at the Nef-induced Lck endosomal compartment colocalizing with Lck (Fig. 3E, 4A). Vav1 is involved in both the TCR-CD3 and CD28 signaling pathways acting as signaling adaptor molecule (47, 48). Moreover, Vav1 is associated with the CD28 intracellular region *via* the signaling adaptor Grb2 (48). CD28 is downregulated during HIV-1 infection in a Nef- and Vpu-dependent manner, inducing CD28 internalization and degradation (5, 49, 50). In agreement with this, we observed that Nef expression induces the accumulation of CD28 in a pericentrosomal compartment that co-localizes with Nef (Fig. 5 A, B). However, we did not find significant co-localization between CD28 and pVav1 in this compartment (Fig. 5C, 5D). In contrast, we observed significant co-localization between intracellularly accumulated

CD28 and Rac1 (Fig. 5E, 5F). This is consistent with the extensive colocalization in the pericentrosomal compartment of Nef and CD28 and of Nef and Rac1). Therefore, Nef-induced pVav1 accumulation in the Nef-induced Lck compartment seems not to be the consequence of recruitment of CD28-associated Vav1, but of a possible soluble fraction. Finally, Vav1 is a regulator (guanine exchange factor, GEF) of Rac1, controlling its activity on actin cytoskeleton dynamics (51). Its accumulation in the Nef-induced Lck compartment under its GEF active form (pTyr174) could be relevant, at least in part for the Nef influence on Rac1 activity.

Altogether, these data show that Nef expression induces the concentration of activation-competent signaling molecules belonging to the TCR signaling pathways, leaving other molecules unperturbed.

Nef does not induce the relocalization of signaling effectors downstream of Lck, TCRζ, ZAP70 and Vav1

We next investigated whether the subcellular localization of signaling proteins downstream of Lck, ZAP70, Vav1 and Rac1 was modified in Nef-expressing cells. To this end, we analyzed the intracellular localization of a number of signaling molecules of the TCR-CD28 signaling pathways leading to the activation of NFAT, NFκB and AP1 (Fos and Jun) transcription factors that together drive T cell differentiation, cytokine production and eventually T cell proliferation (1). Among these downstream signaling proteins, PLCγ1 is activated through Lck and ZAP70-mediated tyrosine phosphorylation to give rise to two key phospholipids second messengers, inositol trisphosphate (IP3) and diacylglycerol (DAG). IP3 regulates calcium flux from the endoplasmic reticulum, while DAG activates protein kinase C (PKC) serine threonine kinases. Increase in intracellular calcium concentration then activates the serine phosphatase calcineurin that dephosphorylates NFAT transcription factor, inducing its translocation to the nucleus. In turn, PKCθ may phosphorylate and activate the kinase Ikkβ, inducing the NFκB signaling pathway and NFκB nuclear translocation. Moreover, binding of Grb2-SOS to phosphorylated LAT facilitates Ras activation and the triggering of the MAP kinase cascade involving Raf, MEK, Erk1/2 and Elk serine/threonine kinases that activate the Fos transcription factor. Finally, Vav1 cooperates with PI3K in the CD28

cosignaling pathway to activate the GTPase Rac1 that in turn activates the Jun kinase (JNK) and the Jun transcription factor (1).

Therefore, we analyzed the effect of Nef-GFP expression in the subcellular localization of proteins and active forms of a number of these key signaling molecules, including Fyn, AKT, pPLCγ1, NEMO, BCL10, CARMA1, mTOR, NF-κB (p105 and p65 subunits), PI3K, PKCθ, pT538-PKCθ, PKCζ, pThr202pY204-Erk1/2, pY185-JNK. We did not find any of these proteins relocalized to the Nef-induced Lck endosomal compartment (Supplementary Fig. S1A-S1D).

These data indicate that Nef effects on the localization of T cell signaling molecules mainly concerns the TCR initiation signaling complex, but does not affect downstream signaling molecules.

Nef-induced accumulation of Lck in the endosomal compartment is concomitant with differential modulation of T cell activation pathways.

The accumulation of signaling competent forms of Lck, TCRζ, ZAP70 and Vav1 suggests that HIV-1 infection may generate *via* Nef an autonomous "endosomal signaling compartment" that delivers constitutive activation signals to the infected T cell. Therefore, we investigated the effect of Nef on activation pathways downstream of those signaling molecules. To this end, we analyzed the expression of a battery of early and late activation genes in T cells infected with HIV-1 WT or Nef-deficient viruses, or in Nef-expressing cells.

Jurkat T cells were infected with HIV-1 WT and ΔNef viruses and RT-qPCR analysis was performed on non-stimulated cells, in order to estimate the potential effects of Nef on constitutive T cell activation, independently of TCR stimulation. Among the genes investigated, the immediate-early activation genes *FOS* and *JUN* (52) were upregulated upon HIV-1 infection with respect to their basal state in cells infected by WT virus, but to a lesser extent in those infected by ΔNef virus (Fig. 6A). In contrast, *MYC* basal expression was equally inhibited by both WT and ΔNef viruses (Fig. 6A). However, the expression of two target genes regulated by the NFκB signaling pathway, IκBα (*NFKBIA*) and TNFα induced protein 3 (*TNFAIP3*) (53, 54) was barely changed (Fig. 6B). In addition, we found the expression of several late T cell activation genes, namely *IL2*, *IL2RA* (CD25) and *IFNG*

(IFNγ), significantly increased in cells infected by HIV-1 WT, and to a lesser extent in those infected with ΔNef viruses (Fig. 6C).

To further investigate whether Nef expression was sufficient to induce those effects, Jurkat cells were transfected with GFP or Nef-GFP expression vectors and sorted by FACS. GFP and Nef-GFP expressing cells were then assayed for their expression of some of the early and late activation genes referred above (Fig. 6D). The activation trend was confirmed, *JUN* and *FOS* were upregulated by Nef, while *TNFAIP3* and *NFKBIA* gene expression were not significantly changed. Finally, no significant variation of *MYC* expression was observed in Nef expressing cells, in agreement with the Nef-independent inhibitory effect of HIV-1 virus infection.

Therefore, HIV-1 infection enhances the expression of several early and late activation genes, in a Nef-dependent manner. The effect of Nef was different from gene to gene, suggesting a variable influence of Nef and other viral proteins.

Nef-induced accumulation of Lck in intracellular compartments is partly neutralized by Rab11-FIP3 depletion and overcomes Nef-induced transcriptional effects

To test whether the activation events induced by HIV-1 Nef were due to the formation of the Nef-induced endosomal Lck compartment, we took advantage of our previous findings showing that Lck is associated with $Rab11^+$ endosomes, whose centripetal movement and localization in the pericentrosomal zone are regulated by the Rab11-FIP3 effector protein (from here on called FIP3) (28). Moreover, modification of Rab11 endosomal traffic by the depletion of FIP3 inhibits Lck-mediated T cell signaling events, even in non-stimulated cells (28). Interestingly, FIP3 overexpression induces Lck intracellular accumulation in a similar fashion than Nef (17, 28). In contrast, FIP3 depletion has the opposite effect, dispersing Rab11 endosomes carrying Lck all over the cytoplasm (28). Therefore, we tested whether FIP3 silencing could overcome Lck intracellular accumulation induced by Nef, as well as its potential functional effects on early and late gene expression.

As observed previously on the Lck pericentrosomal compartment in non-infected cells (28), FIP3 silencing dispersed the Nef-induced Lck/pZAP70 pericentrosomal accumulation, which became more fragmented and spread over the cytoplasm, as assessed by the distribution of Lck and pZAP70 in the pericentrosomal cytoplasmic area (Fig. 7 A, 7B).

We next investigated the effect of FIP3 silencing on HIV-1 Nef-induced upregulation of some of the above-mentioned genes. We used two siRNA oligonucleotides directed to distinct sequences and displaying different silencing efficiencies, siFIP3-2 being more efficient that siFIP3-1 (Fig. 8A top), as we previously reported (28, 31). Note that FIP3 has two isoforms of slightly different electrophoretic mobility (Fig. 8A, double arrow head): siFIP3-1 preferentially silenced, though partially, the one of higher molecular mass, whereas siFIP3-2 silenced both. In cells transfected with si-control, infection with HIV-1 WT viruses led to upregulation of *JUN*, *FOS*, *IFNG* and *IL2*, genes as described above, that was significantly lower in cells infected with Nef-deficient virus (Fig. 8B, 8C). Interestingly, FIP3 silencing counteracted HIV-1-WT-induced gene upregulation reducing the differences between HIV-1 WT and Nef-deficient viruses to lower or non-significant levels in cells silenced with siFIP3-1 and siFIP3-2, respectively (Fig. 8B, 8C, white and grey histogram). Of note is that FIP3 silencing did not alter the percentage of infected cells (Fig. 8D) or Nef levels in cell extracts, but slightly reduced the level of the p24 capsid protein (Fig. 8A, 8D).

These data indicate that: i) the expression of several of the genes analyzed depends in part on the appropriate regulation of the recycling endosomal compartment controlled by Rab11-FIP3; ii) HIV-1 exacerbates the function of this physiological compartment, in a Nef-dependent manner, increasing the expression of these various genes; iii) perturbation of this compartment by FIP3 silencing counteracts, in a dose-dependent manner, the effects of Nef, reducing gene expression of HIV-1-WT-infected cells to the levels of cells infected with Nef-deficient viruses.

Nef sequesters Rac1 in its intracellular compartment and modulates Rac1-mediated T cell spreading

In addition to Lck and several of its substrates, we found the GTPase Rac1 concentrated in a pericentrosomal compartment in a Nef-dependent fashion (Fig. 1 B, D). To better define the intracellular compartment in which Nef retains Rac1, we expressed Nef-GFP in Jurkat and primary $CD4^+$ T cells and analyzed its relative localization to endogenous Rac1. In control cells expressing GFP, Rac1 is localized at the plasma membrane, in the cytosol, and to a lesser extent in pericentrosomal endosomes, likely corresponding to $Rab11^+$ endosomes, as we previously described (31) (Fig. 9A top). In Nef-GFP expressing cells, Rac1 was massively localized in an intracellular compartment that extensively colocalized with Nef (Fig. 9A bottom, 9C). Similar results were found in primary human $CD4^+$ T cells transfected with Nef-

GFP (Fig. 9B, 9C), although the intracellular compartment was less well spatially resolved due to the smaller cytoplasmic volume of primary T cells.

T cell membrane protrusions formed during T cell spreading and immunological synapse formation are reminiscent of lamellipodium structures observed in migrating cells (55), whose formation depends on Rac1 (56). Moreover, we have recently shown that Rac1 is associated with $Rab11^+$ endosomes and its subcellular localization is controlled by FIP3. Thus, FIP3-silenced T cells lose the Rac1/Rab11 pericentrosomal compartment, which gets fragmented and spreads all over the cytoplasm. Conversely, FIP3 overexpression induces the accumulation of Rac1 in the $Rab11^+$ pericentrosomal compartment (31), somehow reminiscent of Nef effect on Rac1 intracellular localization (Fig. 2C, 9A, 9B). Rab11-mediated Rac1 traffic controls Rac1 functions in T cells. In particular, we showed that T cell capacity to spread on surfaces was exacerbated, both in the presence and absence of TCR stimulation or integrin adhesion (i.e. T cells spreading on poly-lysine). Therefore, we analyzed to what extent FIP3 silencing could compensate Nef-induced Rac1 concentration in the pericentrosomal compartment, and whether Nef was still capable to sequester Rac1 in FIP3-silenced cells. We observed that Rac1 intracellular dispersion in FIP3-silenced / Nef-expressing cells was less efficient than the one we previously observed in control cells not expressing Nef (31), and did not significantly altered Nef and Rac1 colocalization (Fig. 9D-9F).

We then investigated whether Nef has an effect on T cells spreading on poly-lysine, which we showed was enhanced in FIP3-silenced cells (31). Therefore, we transfected Jurkat T cells with GFP or Nef-GFP together with si-control or siFIP3 oligonucleotides and analyzed the capacity of cells to spread on poly-lysine. We used poly-lysine as adhesion substrate in order to analyze the effects due to Rac1 and not those potentially involving Lck signaling in T cells spreading on anti-CD3, a process reported to be affected by Nef (10). We observed that Nef expression did not have a significant effect on si-control-treated T cell spreading on poly-lysine, but significantly inhibited the enhancing effect of FIP3 silencing, especially at late times (Fig. 9G, 9H, 15 min).

Altogether, these data indicate that the Nef subversion of Rac1 endosomal traffic and Rac1 sequestering in the Nef intracellular compartment modulates Rac1-mediated actin remodeling that supports TCR signaling-independent T cell spreading.

Discussion

Under physiological conditions, the endosomal traffic of TCR and several of its proximal signaling molecules is crucial for immunological synapse formation and T cell activation. At least three main functions for this molecular traffic have been proposed: first, the targeting of TCR and signaling molecules to the immunological synapse allowing the generation of signaling complexes at the synaptic plasma membrane (2, 20, 21, 23, 25, 26, 30, 57); second, the delivery of signaling complexes to endosomes to sustain T cell activation (58); third, the removal of TCRs and signaling molecules from the synaptic plasma membrane in order to down regulate T cell activation (59-61). During HIV-1 infection, the viral protein Nef appears to specifically hijack some of these endosomal pathways, perturbing Lck intracellular traffic with several opposite effects reported: first, to limit Lck clustering and tyrosine phosphorylation of signaling adaptors at the immunological synapse (17, 18); second, to increase the sensitivity of the Ras-Erk and calcium signaling pathways leading to NFAT activation and IL2 production in response to TCR and CD28 stimulation (16, 19, 62-67). The influence of HIV-1 infection and Nef expression on other components of the T cell activation molecular machinery remains, however, poorly defined.

Here, we show that HIV-1 infection induces the accumulation of Lck and Rac1 in a pericentrosomal vesicular compartment. Nef is necessary to induce this double accumulation, but the differences between WT and ΔNef infected cells do not allow us to ensure a full dependence on Nef expression. Other viral proteins might also be involved. Nevertheless, Nef expression alone is enough to induce these effects. Indeed, Nef appears to finely assemble an "autonomous endosomal signaling compartment" that gathers activation-competent forms (i.e. phosphorylated at key Tyr residues) of several TCR-CD3 and CD28 proximal signaling molecules. This compartment includes the phosphorylated active form of Lck, together with pTCRζ, pZAP70, pSLP76 and pVav1, but not pLAT. Interestingly, Lck, TCRζ and LAT are associated with spatially adjacent but distinct endosomal compartments (21, 25, 26, 28), while, ZAP70, SLP76 and Vav1 are not associated with endosomes (68) (and our unpublished data). Therefore, the Nef-induced signaling compartment seems not to be just the consequence of the general perturbation of endosomal traffic. Rather, our data are consistent with Nef specifically altering Lck and TCRζ endosomal traffic, concentrating both proteins in pericentrosomal endosomes, and favoring TCRζ phosphorylation. In addition, the reported

interactions of Nef with Lck (69) and TCRζ (70) might also contribute to generate this compartment. In turn, locally phosphorylated TCRζ, would bind ZAP70, favoring its concentration in that compartment, ZAP70 autophosphorylation, and ZAP70 phosphorylation and activation by Lck (4). It is tempting to speculate that Nef could stabilize a transient physiological intermediate signaling compartment (58) providing steady activation signals to the infected cell. To test this hypothesis, we crosslinked CD3 and CD28 and followed the potential generation of an enhanced Lck endosomal compartment containing phosphorylated Lck substrates. We could not detect increased accumulation of Lck or pZAP70 in the pericentrosomal area at activation time points between 5 and 30 min in which pZAP70 and TCRζ phosphorylation occurs (28), together with TCR-CD3 internalization (20), (Supplemental Fig. 2A, 2B). Rather, the Lck endosomal compartment appeared to lose intensity, as we previously reported (25). This indicates that a translocation of Lck to the plasma membrane occurs, instead of Lck endosomal enrichment.

In contrast to what occurs at the immunological synapse plasma membrane, endosome-associated active ZAP70 seems not to be able to phosphorylate endosomal LAT. Nevertheless, pSLP76 concentrates there. Therefore, pSLP76 recruitment to the Nef-induced signaling compartment would not occur *via* pLAT (3). The lack of local formation of optimal amplification complex formed by pLAT and pSLP76 (3) may explain why the constitutive activation of genes induced by Nef is relatively weak (1.5-4 fold higher than the expression of non-infected cells), as compared with that induced by TCR-CD28 stimulation, which generally leads to higher gene expression levels (4-100 fold higher than the expression of non-stimulated cells (28). Instead of pLAT, the interaction of SLP76 with Vav1 (71) could account for SLP76 recruitment, but how these two molecules are recruited remains unknown. It has been reported that Nef interacts with Vav1 in cholesterol and sphingolipids-enriched (detergent insoluble) membrane microdomains (8, 9, 11). These membrane microdomains also continuously cycle between the plasma membrane and the endosomal compartment and could help Vav1 concentration in the pericentrosomal region close to Lck. It is tempting to speculate that while TCR + CD28 induce a strong response leading to proliferation, Nef does not generate a proliferation signal, but rather a mild survival signal that may favor virus replication.

The kinetics of Lck and Rac1 accumulation in the pericentrosomal compartment upon HIV-1 infection remain not resolved. The difficulty to detect low levels of Nef expression by immunofluorescence and confocal microscopy, together with intrinsic variability of Lck and

552 Rac1 concentration in the pericentrosomal compartment in non-infected cells make these
553 quantitative measurements at present poorly reliable (our unpublished data).

554 We have identified several early and late activation genes that are differentially
555 regulated during HIV-1 infection in a partly Nef-dependent fashion, even in the absence of
556 TCR stimulation. Thus, *FOS* and *JUN* were upregulated by HIV-1 infection, in a partly Nef-
557 dependent manner. In contrast, *MYC* expression was inhibited, although in a Nef-independent
558 manner. Finally, *NFKBIA* and *TNFAIP3* remained non-significantly changed. This is
559 consistent with previous reports proposing a Nef-mediated modulation of the Ras-Erk,
560 calcium and NFAT signaling pathway with no effect on NF-κB (19, 62-64, 72). In addition,
561 we observed that several late activation genes, like *IL2, IL2RA* and *IFNG* were upregulated in
562 HIV-1 infected cells in a partly Nef-dependent manner. The extent of upregulation and Nef
563 dependence varies among the different genes, suggesting that other HIV-1 proteins may
564 contribute to these effects by this or different mechanisms. Further evidence for Nef
565 dependency of HIV-1-infected cells was the observations that Nef expression by itself
566 increased *JUN* and *FOS* gene expression, without affecting *MYC*, *NFKBIA* and *TNFAIP3*.

567 While our data herein show that HIV-1 infection increases the expression of these
568 various genes independently of TCR stimulation, other authors have shown that Nef
569 expression enhances TCR-CD28 stimulation (16, 19, 62-67). In our case, we cannot rule out
570 that TCR-independent co-stimulation *via* T cell-T cell interaction occurs and contributes to
571 the observed effects. Under physiological conditions, infected cells might get mild
572 stimulations from other cells in lymphoid organs that may cooperate with the Nef-induced
573 compartment to activate infected cells.

574 We have previously shown that Rab11 endosomal traffic is key for Lck and Rac1
575 regulatory functions in T cells. This mechanism modulates TCR signaling and Rac1-mediated
576 actin cytoskeleton remodeling, both important during immunological synapse formation and
577 T cell activation leading to cytokine production (28, 31, 32). Interestingly, Nef mimics FIP3
578 overexpression in its ability to accumulate Lck and Rac1 in the pericentrosomal compartment.
579 The resemblance of effects of Nef and FIP3 overexpression on Lck and Rac1 endosomal
580 traffic is striking and suggest a common mechanism involving Rab11-driven endosomal
581 traffic. For instance, both proteins affect transferrin and transferrin receptor endosomal traffic
582 (34, 73). Moreover, both proteins interact with members of the exocyst complex that regulates
583 vesicle tethering to the plasma membrane and may affect endosomal traffic (74, 75).
584 Conversely, Nef has the opposite effect of FIP3 silencing, enhancing the phosphorylation of

some Lck substrates, and counteracting the effect of FIP3 silencing on T cell spreading. Altogether, these data indicate that Nef hijacks the endosomal traffic of Lck and Rac1 to modulate, in an opposite manner, signaling- and actin cytoskeleton-mediated T cell functions. This combined mechanisms may account in part for the reported multiple and sometimes contradictory effects of HIV-1 infection and Nef expression on T cell activation (16), as well as Nef effects on T cell actin cytoskeleton, influencing T cell spreading, cell shape changes and migration (9, 10, 13, 14, 76). Additionally, the Nef effects we describe here may complement other reported mechanisms involving Nef interactions with some signaling and cytoskeleton regulators (16). Finally, Pan et al (19) reported that Nef-induced intracellular retention of Lck could be counteracted by the overexpression of Unc119, a protein also involved in Lck traffic *via* the Rab11 endosomal compartment and in Lck activation (22, 77), further supporting the effect of Rab11 traffic in the effects of Nef on Lck.

FIP3 silencing affects gene expression in both non-infected and HIV-1-infected cells and balances the differences between cells infected with HIV-1 WT and Nef-deficient viruses. This is consistent with the idea that HIV-1 hijacks *via* Nef signaling mechanisms existing in non-infected T cells, exacerbating them to produce higher basal levels of some transcription factors (i.e. Fos and Jun) and cytokines (i.e. IFNγ and IL2). This may contribute to an equilibrium between the virus and the infected cell favoring virus replication. In this line, Nef-induced modulation of T cell endosomal and Lck traffic was reported to contribute to virus replication (19, 34). Finally, the subtle relocalization of part of the TCR and CD28 signaling machinery might be important for specific HIV-1 effects on apoptosis, or in the process of reprogramming infected cells to quiescence, but this will need further investigation (78).

We observed that Nef recruits Rac1 in a compartment that overlaps and colocalizes with Nef more extensively than Lck and the other recruited signaling molecules. This is consistent with an interaction between Nef and Rac1 as shown by others (11, 79). Rac1 and its GEF activator Vav1 have two related functions in T cells, to transduce TCR and CD28 activation signals and to regulate actin cytoskeleton dynamics. In this line, previous reports proposed that Vav1 and Rac1 are involved in Nef-mediated activation of PAK2 (8, 11) and may enhance Ras-Erk and JNK signaling pathways (9, 64). In some of these reports, detergent-insoluble membrane microdomains were suggested to be involved but the two mechanisms would not be exclusive, since membrane microdomains transit through recycling endosomes. Interestingly, we did not observe relocalization of active-phosphorylated forms of Erk or

JNK. However, according to the above-cited reports, these kinases are more prone to be activated in Nef-expressing cells when the TCR is engaged. Therefore, we could speculate that the Nef-induced endosomal signaling compartment facilitates the delivery of activation signals to these kinases without concentrating them in this compartment, and leading to increase transcription of cytokine genes, as we show here.

We could not elucidate in our study whether Nef can relocalize other Rho-family GTPases, as Rho and Cdc42, because of lack of performing antibodies able to detect endogenous proteins. Worth noting, Rauch et al. reported that Rac1, Cdc42 and Vav1 are recruited to Nef-PAK2 complexes within detergent-insoluble membrane microdomains. They proposed that this recruitment may contribute to Nef effects on T cell activation (11). However, the subcellular localization of the reported complexes appears very different than the Rac1-Nef co-recruitment we describe here. Our data indicate that Rac1 sequestering by Nef is inhibitory for Rac1-mediated cytoskeletal rearrangements leading to T cell spreading. This could also explain the modulatory effect of Nef on T cell shape and migration reported by others (12-14, 76). Therefore, different localizations of Rac1 with respect to Nef might lead to distinct opposite effects. Localization in membrane microdomains might favor signaling, whereas endosomal sequestering might have a dual effect, enhance the Vav1-Rac1 signaling pathway and inhibit Rac1-mediated actin cytoskeleton reorganization, as shown here on T cell spreading.

In conclusion, this work provides new insights into the understanding of HIV-1 host T cell interactions, *via* the subtle modulation of the endosomal traffic of signaling and cytoskeleton regulators. The two mechanisms are likely different and lead to opposite outputs. Our findings may be the reflect of Nef effects at various steps of the virus life cycle: first, during early phases of infection, in which virus-borne Nef enters the target cell and may cause subcellular local effects on signaling or cytoskeleton; second, during HIV-1 genome transcription in which Nef is expressed from the integrated viral genome, causing more general effects in the infected cells together with other viral proteins; third, Nef could affect bystander cells to which it could be transferred from infected cells, causing Nef specific effects. Finally, although our work largely focused on Nef-dependent effects, our data show that other viral proteins may have significant effects on T cell signaling, using perhaps complementary mechanisms. Finally, Nef induced reorganization of the recycling endosomal compartment an as a consequence the proteins transported by these endosomes, may contribute to the effect of Nef in virus replication as indicated by previous reports (19, 34).

Acknowledgments

We thank the Photonic BioImaging UTechS microscopy core facility at the Institut Pasteur for microscopy and technical support, the Cytometry and Biomarkers UTechS core facility at the Institut Pasteur for flow cytometry, cell sorting and technical support, the French Blood Bank (Etablissement Francais du Sang) and the ICAReB (Clinical Investigation and Access to Biological Resources core facility) team for providing blood from healthy donors and primary T cell samples, respectively. The following reagents were obtained through the NIH AIDS Reagent Program, Division of AIDS, NIAID, NIH: monoclonal antibody to HIV-1 p24 (AG3.0) from Dr. Jonathan Allan (80); anti-HIV-1 Nef monoclonal (6.2) from Dr. Kai Krohn and Dr. Vladimir Ovod (81) and HIV-1SF2 p24 antiserum from DAIDS, NIAID, produced by BioMolecular Technologies. We thank Drs S. Benichou and F. Niedergang (Institut Cochin, Paris); H. Moreaux, A. M. Lennon-Dumenil and S. Agüera-Gonzalez (Institut Curie, Paris); and A. Echard, R. Weil and S. Etienne-Manneville (Institut Pasteur, Paris) for antibodies, expression vectors, and methodological help and advice.

Disclosures

The authors have no financial conflict of interest

References

1. Agüera-Gonzalez, S., J. Bouchet, and A. Alcover. 2015. Immunological Synapse. *eLS. John Wiley & Sons, Ltd: Chichester* DOI: 10.1002/9780470015902.a0004027.pub2.
2. Niedergang, F., V. Di Bartolo, and A. Alcover. 2016. Comparative anatomy of phagocytic and immunological synapses. *Front Immunol* 7: 18 doi 10.3389/fimmu.2016.00018.
3. Acuto, O., V. D. Bartolo, and F. Michel. 2008. Tailoring T-cell receptor signals by proximal negative feedback mechanisms. *Nat Rev Immunol* 8: 699-712.
4. Malissen, B., and P. Bongrand. 2015. Early T cell activation: integrating biochemical, structural, and biophysical cues. *Annu Rev Immunol* 33: 539-561.
5. Pereira, E. A., and L. L. daSilva. 2016. HIV-1 Nef: Taking Control of Protein Trafficking. *Traffic* 17: 976-996.
6. Lehmann, M., D. S. Nikolic, and V. Piguet. 2011. How HIV-1 takes advantage of the cytoskeleton during replication and cell-to-cell transmission. *Viruses* 3: 1757-1776.
7. Verollet, C., V. Le Cabec, and I. Maridonneau-Parini. 2015. HIV-1 Infection of T Lymphocytes and Macrophages Affects Their Migration via Nef. *Front Immunol* 6: 514.
8. Fackler, O. T., X. Lu, J. A. Frost, M. Geyer, B. Jiang, W. Luo, A. Abo, A. S. Alberts, and B. M. Peterlin. 2000. p21-activated kinase 1 plays a critical role in cellular activation by Nef. *Mol Cell Biol* 20: 2619-2627.
9. Fackler, O. T., W. Luo, M. Geyer, A. S. Alberts, and B. M. Peterlin. 1999. Activation of Vav by Nef induces cytoskeletal rearrangements and downstream effector functions. *Mol Cell* 3: 729-739.
10. Haller, C., S. Rauch, N. Michel, S. Hannemann, M. J. Lehmann, O. T. Keppler, and O. T. Fackler. 2006. The HIV-1 pathogenicity factor Nef interferes with maturation of stimulatory T-lymphocyte contacts by modulation of N-Wasp activity. *J Biol Chem* 281: 19618-19630.
11. Rauch, S., K. Pulkkinen, K. Saksela, and O. T. Fackler. 2008. Human immunodeficiency virus type 1 Nef recruits the guanine exchange factor Vav1 via an unexpected interface into plasma membrane microdomains for association with p21-activated kinase 2 activity. *J Virol* 82: 2918-2929.
12. Stolp, B., L. Abraham, J. M. Rudolph, and O. T. Fackler. 2010. Lentiviral Nef proteins utilize PAK2-mediated deregulation of cofilin as a general strategy to interfere with actin remodeling. *J Virol* 84: 3935-3948.
13. Stolp, B., M. Reichman-Fried, L. Abraham, X. Pan, S. I. Giese, S. Hannemann, P. Goulimari, E. Raz, R. Grosse, and O. T. Fackler. 2009. HIV-1 Nef interferes with host cell motility by deregulation of Cofilin. *Cell Host Microbe* 6: 174-186.
14. Nobile, C., D. Rudnicka, M. Hasan, N. Aulner, F. Porrot, C. Machu, O. Renaud, M. C. Prevost, C. Hivroz, O. Schwartz, and N. Sol-Foulon. 2010. HIV-1 Nef inhibits ruffles, induces filopodia, and modulates migration of infected lymphocytes. *J Virol* 84: 2282-2293.
15. Abraham, L., and O. T. Fackler. 2012. HIV-1 Nef: a multifaceted modulator of T cell receptor signaling. *Cell Commun Signal* 10: 39.
16. Markle, T. J., M. Philip, and M. A. Brockman. 2013. HIV-1 Nef and T-cell activation: a history of contradictions. *Future Virol* 8.
17. Thoulouze, M. I., N. Sol-Foulon, F. Blanchet, A. Dautry-Varsat, O. Schwartz, and A. Alcover. 2006. Human immunodeficiency virus type-1 infection impairs the formation of the immunological synapse. *Immunity* 24: 547-561.
18. Abraham, L., P. Bankhead, X. Pan, U. Engel, and O. T. Fackler. 2012. HIV-1 Nef Limits Communication between Linker of Activated T Cells and SLP-76 To Reduce

Formation of SLP-76-Signaling Microclusters following TCR Stimulation. *J Immunol* 189: 1898-1910.
19. Pan, X., J. M. Rudolph, L. Abraham, A. Habermann, C. Haller, J. Krijnse-Locker, and O. T. Fackler. 2012. HIV-1 Nef compensates for disorganization of the immunological synapse by inducing trans-Golgi network-associated Lck signaling. *Blood* 119: 786-797.
20. Das, V., B. Nal, A. Dujeancourt, M. I. Thoulouze, T. Galli, P. Roux, A. Dautry-Varsat, and A. Alcover. 2004. Activation-induced polarized recycling targets T cell antigen receptors to the immunological synapse; involvement of SNARE complexes. *Immunity* 20: 577-588.
21. Anton, O., A. Batista, J. Millan, L. Andres-Delgado, R. Puertollano, I. Correas, and M. A. Alonso. 2008. An essential role for the MAL protein in targeting Lck to the plasma membrane of human T lymphocytes. *J Exp Med* 205: 3201-3213.
22. Gorska, M. M., Q. Liang, Z. Karim, and R. Alam. 2009. Uncoordinated 119 protein controls trafficking of Lck via the Rab11 endosome and is critical for immunological synapse formation. *J Immunol* 183: 1675-1684.
23. Finetti, F., S. R. Paccani, M. G. Riparbelli, E. Giacomello, G. Perinetti, G. J. Pazour, J. L. Rosenbaum, and C. T. Baldari. 2009. Intraflagellar transport is required for polarized recycling of the TCR/CD3 complex to the immune synapse. *Nat Cell Biol* 11: 1332-1339.
24. Anton, O. M., L. Andres-Delgado, N. Reglero-Real, A. Batista, and M. A. Alonso. 2011. MAL Protein Controls Protein Sorting at the Supramolecular Activation Cluster of Human T Lymphocytes. *J Immunol* 186: 6345-6356.
25. Soares, H., R. Henriques, M. Sachse, L. Ventimiglia, M. A. Alonso, C. Zimmer, M. I. Thoulouze, and A. Alcover. 2013. Regulated vesicle fusion generates signaling nanoterritories that control T cell activation at the immunological synapse. *J Exp Med* 210: 2415-2433.
26. Larghi, P., D. J. Williamson, J. M. Carpier, S. Dogniaux, K. Chemin, A. Bohineust, L. Danglot, K. Gaus, T. Galli, and C. Hivroz. 2013. VAMP7 controls T cell activation by regulating the recruitment and phosphorylation of vesicular Lat at TCR-activation sites. *Nat Immunol* 14: 723-731.
27. Finetti, F., L. Patrussi, D. Galgano, C. Cassioli, G. Perinetti, G. J. Pazour, and C. T. Baldari. 2015. The small GTPase Rab8 interacts with VAMP-3 to regulate the delivery of recycling T-cell receptors to the immune synapse. *J Cell Sci* 128: 2541-2552.
28. Bouchet, J., I. Del Rio-Iniguez, E. Vazquez-Chavez, R. Lasserre, S. Aguera-Gonzalez, C. Cuche, M. W. McCaffrey, V. Di Bartolo, and A. Alcover. 2017. Rab11-FIP3 Regulation of Lck Endosomal Traffic Controls TCR Signal Transduction. *J Immunol* 198: 2967-2978.
29. Pfisterer, K., F. Forster, W. Paster, V. Supper, A. Ohradanova-Repic, P. Eckerstorfer, A. Zwirzitz, C. Donner, C. Boulegue, H. B. Schiller, G. Ondrovicova, O. Acuto, H. Stockinger, and V. Leksa. 2014. The late endosomal transporter CD222 directs the spatial distribution and activity of Lck. *J Immunol* 193: 2718-2732.
30. Carpier, J. M., A. E. Zucchetti, L. Bataille, S. Dogniaux, M. Shafaq-Zadah, S. Bardin, M. Lucchino, M. Maurin, L. D. Joannas, J. G. Magalhaes, L. Johannes, T. Galli, B. Goud, and C. Hivroz. 2018. Rab6-dependent retrograde traffic of LAT controls immune synapse formation and T cell activation. *J Exp Med*.
31. Bouchet, J., I. Del Rio-Iniguez, R. Lasserre, S. Aguera-Gonzalez, C. Cuche, A. Danckaert, M. W. McCaffrey, V. Di Bartolo, and A. Alcover. 2016. Rac1-Rab11-FIP3

771 regulatory hub coordinates vesicle traffic with actin remodeling and T-cell activation.
772 *EMBO J* 35: 1160-1174.
773 32. Bouchet, J., M. W. McCaffrey, A. Graziani, and A. Alcover. 2016. The functional
774 interplay of Rab11, FIP3 and Rho proteins on the endosomal recycling pathway
775 controls cell shape and symmetry. *Small GTPases*: 1-6.
776 33. Greenberg, M. E., A. J. Iafrate, and J. Skowronski. 1998. The SH3 domain-binding
777 surface and an acidic motif in HIV-1 Nef regulate trafficking of class I MHC
778 complexes. *EMBO J* 17: 2777-2789.
779 34. Madrid, R., K. Janvier, D. Hitchin, J. Day, S. Coleman, C. Noviello, J. Bouchet, A.
780 Benmerah, J. Guatelli, and S. Benichou. 2005. Nef-induced alteration of the
781 early/recycling endosomal compartment correlates with enhancement of HIV-1
782 infectivity. *J Biol Chem* 280: 5032-5044.
783 35. Craig, H. M., M. W. Pandori, and J. C. Guatelli. 1998. Interaction of HIV-1 Nef with
784 the cellular dileucine-based sorting pathway is required for CD4 down-regulation and
785 optimal viral infectivity. *Proc. Natl Acad. Sci. USA* 95: 11229-11234.
786 36. Spina, C. A., T. J. Kwoh, M. Y. Chowers, J. C. Guatelli, and D. D. Richman. 1994.
787 The importance of nef in the induction of human immunodeficiency virus type 1
788 replication from primary quiescent CD4 lymphocytes. *J Exp Med* 179: 115-123.
789 37. Stewart, S. A., D. M. Dykxhoorn, D. Palliser, H. Mizuno, E. Y. Yu, D. S. An, D. M.
790 Sabatini, I. S. Chen, W. C. Hahn, P. A. Sharp, R. A. Weinberg, and C. D. Novina.
791 2003. Lentivirus-delivered stable gene silencing by RNAi in primary cells. *RNA* 9:
792 493-501.
793 38. Bouchet, J., I. Del Rio-Iniguez, and A. Alcover. 2017. Imaging Vesicular Traffic at
794 the Immune Synapse. *Methods in molecular biology* 1584: 129-142.
795 39. Del Rio-Iniguez, I., J. Bouchet, and A. Alcover. 2017. Studying the Immune Synapse
796 in HIV-1 Infection. *Methods in molecular biology* 1584: 545-557.
797 40. Schindelin, J., I. Arganda-Carreras, E. Frise, V. Kaynig, M. Longair, T. Pietzsch, S.
798 Preibisch, C. Rueden, S. Saalfeld, B. Schmid, J. Y. Tinevez, D. J. White, V.
799 Hartenstein, K. Eliceiri, P. Tomancak, and A. Cardona. 2012. Fiji: an open-source
800 platform for biological-image analysis. *Nat Methods* 9: 676-682.
801 41. Bolte, S., and F. P. Cordelieres. 2006. A guided tour into subcellular colocalization
802 analysis in light microscopy. *J Microsc* 224: 213-232.
803 42. Costes, S. V., D. Daelemans, E. H. Cho, Z. Dobbin, G. Pavlakis, and S. Lockett. 2004.
804 Automatic and quantitative measurement of protein-protein colocalization in live cells.
805 *Biophysical journal* 86: 3993-4003.
806 43. Pan, X., M. M. Geist, J. M. Rudolph, W. Nickel, and O. T. Fackler. 2013. HIV-1 Nef
807 disrupts membrane-microdomain-associated anterograde transport for plasma
808 membrane delivery of selected Src family kinases. *Cell Microbiol* 15: 1605-1621.
809 44. Kelly, E. E., C. P. Horgan, and M. W. McCaffrey. 2012. Rab11 proteins in health and
810 disease. *Biochem Soc Trans* 40: 1360-1367.
811 45. Nika, K., C. Soldani, M. Salek, W. Paster, A. Gray, R. Etzensperger, L. Fugger, P.
812 Polzella, V. Cerundolo, O. Dushek, T. Hofer, A. Viola, and O. Acuto. 2010.
813 Constitutively active Lck kinase in T cells drives antigen receptor signal transduction.
814 *Immunity* 32: 766-777.
815 46. Haller, C., S. Rauch, and O. T. Fackler. 2007. HIV-1 Nef employs two distinct
816 mechanisms to modulate Lck subcellular localization and TCR induced actin
817 remodeling. *PLoS ONE* 2: e1212.
818 47. Michel, F., G. Mangino, G. Attal-Bonnefoy, L. Tuosto, A. Alcover, A. Roumier, D.
819 Olive, and O. Acuto. 2000. CD28 utilizes Vav-1 to enhance TCR-proximal signaling
820 and NF-AT activation. *J Immunol* 165: 3820-3829.

48. Boomer, J. S., and J. M. Green. 2010. An enigmatic tail of CD28 signaling. *Cold Spring Harb Perspect Biol* 2: a002436.
49. Swigut, T., N. Shohdy, and J. Skowronski. 2001. Mechanism for down-regulation of CD28 by Nef. *EMBO J* 20: 1593-1604.
50. Pawlak, E. N., B. S. Dirk, R. A. Jacob, A. L. Johnson, and J. D. Dikeakos. 2018. The HIV-1 accessory proteins Nef and Vpu downregulate total and cell surface CD28 in CD4(+) T cells. *Retrovirology* 15: 6.
51. Hornstein, I., A. Alcover, and S. Katzav. 2004. Vav proteins, masters of the world of cytoskeleton organization. *Cell Signal* 16: 1-11.
52. Chauhan, D., S. M. Kharbanda, E. Rubin, B. A. Barut, A. Mohrbacher, D. W. Kufe, and K. C. Anderson. 1993. Regulation of c-jun gene expression in human T lymphocytes. *Blood* 81: 1540-1548.
53. Rao, N. A., M. T. McCalman, P. Moulos, K. J. Francoijs, A. Chatziioannou, F. N. Kolisis, M. N. Alexis, D. J. Mitsiou, and H. G. Stunnenberg. 2011. Coactivation of GR and NFKB alters the repertoire of their binding sites and target genes. *Genome research* 21: 1404-1416.
54. Altonsy, M. O., S. K. Sasse, T. L. Phang, and A. N. Gerber. 2014. Context-dependent cooperation between nuclear factor kappaB (NF-kappaB) and the glucocorticoid receptor at a TNFAIP3 intronic enhancer: a mechanism to maintain negative feedback control of inflammation. *J Biol Chem* 289: 8231-8239.
55. Dustin, M. L. 2007. Cell adhesion molecules and actin cytoskeleton at immune synapses and kinapses. *Curr Opin Cell Biol* 19: 529-533.
56. Rougerie, P., and J. Delon. 2012. Rho GTPases: masters of T lymphocyte migration and activation. *Immunology letters* 142: 1-13.
57. Purbhoo, M. A., H. Liu, S. Oddos, D. M. Owen, M. A. Neil, S. V. Pageon, P. M. French, C. E. Rudd, and D. M. Davis. 2010. Dynamics of subsynaptic vesicles and surface microclusters at the immunological synapse. *Sci Signal* 3: ra36.
58. Yudushkin, I. A., and R. D. Vale. 2010. Imaging T-cell receptor activation reveals accumulation of tyrosine-phosphorylated CD3zeta in the endosomal compartment. *Proc Natl Acad Sci U S A* 107: 22128-22133.
59. Alcover, A., B. Alarcon, and V. Di Bartolo. 2017. Cell Biology of T Cell Receptor Expression and Regulation. *Annu Rev Immunol*.
60. Balagopalan, L., V. A. Barr, C. L. Sommers, M. Barda-Saad, A. Goyal, M. S. Isakowitz, and L. E. Samelson. 2007. c-Cbl-mediated regulation of LAT-nucleated signaling complexes. *Mol Cell Biol* 27: 8622-8636.
61. Barr, V. A., L. Balagopalan, M. Barda-Saad, R. Polishchuk, H. Boukari, S. C. Bunnell, K. M. Bernot, Y. Toda, R. Nossal, and L. E. Samelson. 2006. T-cell antigen receptor-induced signaling complexes: internalization via a cholesterol-dependent endocytic pathway. *Traffic* 7: 1143-1162.
62. Manninen, A., G. H. Renkema, and K. Saksela. 2000. Synergistic activation of NFAT by HIV-1 nef and the Ras/MAPK pathway. *J Biol Chem* 275: 16513-16517.
63. Manninen, A., and K. Saksela. 2002. HIV-1 Nef interacts with inositol trisphosphate receptor to activate calcium signaling in T cells. *J Exp Med* 195: 1023-1032.
64. Schrager, J. A., V. Der Minassian, and J. W. Marsh. 2002. HIV Nef increases T cell ERK MAP kinase activity. *J Biol Chem* 277: 6137-6142.
65. Witte, V., B. Laffert, O. Rosorius, P. Lischka, K. Blume, G. Galler, A. Stilper, D. Willbold, P. D'Aloja, M. Sixt, J. Kolanus, M. Ott, W. Kolanus, G. Schuler, and A. S. Baur. 2004. HIV-1 Nef mimics an integrin receptor signal that recruits the polycomb group protein Eed to the plasma membrane. *Mol Cell* 13: 179-190.

66. Schrager, J. A., and J. W. Marsh. 1999. HIV-1 Nef increases T cell activation in a stimulus-dependent manner. *Proc Natl Acad Sci U S A* 96: 8167-8172.
67. Wang, J. K., E. Kiyokawa, E. Verdin, and D. Trono. 2000. The Nef protein of HIV-1 associates with rafts and primes T cells for activation. *Proc Natl Acad Sci U S A* 97: 394-399.
68. Groysman, M., I. Hornstein, A. Alcover, and S. Katzav. 2002. Vav-1 and Ly-GDI, two regulators of Rho GTPases, function cooperatively as signal transducers in T cell antigen receptor-induced pathways. *J. Biol. Chem.* 277: 50121-50130.
69. Collette, Y., H. Dutartre, A. Benziane, M. Ramos, R. Benarous, M. Harris, and D. Olive. 1996. Physical and functional interaction of Nef with Lck.HIV-1 Nef-induced T cell signaling defects. *J. Biol. Chem.* 271: 6333-6341.
70. Xu, X. N., B. Laffert, G. R. Screaton, M. Kraft, D. Wolf, W. Kolanus, J. Mongkolsapay, A. J. McMichael, and A. S. Baur. 1999. Induction of Fas ligand expression by HIV involves the interaction of Nef with the T cell receptor zeta chain. *J Exp Med* 189: 1489-1496.
71. Ksionda, O., A. Saveliev, R. Kochl, J. Rapley, M. Faroudi, J. E. Smith-Garvin, C. Wulfing, K. Rittinger, T. Carter, and V. L. Tybulewicz. 2012. Mechanism and function of Vav1 localisation in TCR signalling. *J Cell Sci* 125: 5302-5314.
72. Witte, V., B. Laffert, P. Gintschel, E. Krautkramer, K. Blume, O. T. Fackler, and A. S. Baur. 2008. Induction of HIV transcription by Nef involves Lck activation and protein kinase C theta raft recruitment leading to activation of ERK1/2 but not NF kappa B. *J Immunol* 181: 8425-8432.
73. Horgan, C. P., A. Oleksy, A. V. Zhdanov, P. Y. Lall, I. J. White, A. R. Khan, C. E. Futter, J. G. McCaffrey, and M. W. McCaffrey. 2007. Rab11-FIP3 is critical for the structural integrity of the endosomal recycling compartment. *Traffic* 8: 414-430.
74. Fielding, A. B., E. Schonteich, J. Matheson, G. Wilson, X. Yu, G. R. Hickson, S. Srivastava, S. A. Baldwin, R. Prekeris, and G. W. Gould. 2005. Rab11-FIP3 and FIP4 interact with Arf6 and the exocyst to control membrane traffic in cytokinesis. *EMBO J* 24: 3389-3399.
75. Mukerji, J., K. C. Olivieri, V. Misra, K. A. Agopian, and D. Gabuzda. 2012. Proteomic analysis of HIV-1 Nef cellular binding partners reveals a role for exocyst complex proteins in mediating enhancement of intercellular nanotube formation. *Retrovirology* 9: 33.
76. Stolp, B., A. Imle, F. M. Coelho, M. Hons, R. Gorina, R. Lyck, J. V. Stein, and O. T. Fackler. 2012. HIV-1 Nef interferes with T-lymphocyte circulation through confined environments in vivo. *Proc Natl Acad Sci U S A* 109: 18541-18546.
77. Gorska, M. M., S. J. Stafford, O. Cen, S. Sur, and R. Alam. 2004. Unc119, a novel activator of Lck/Fyn, is essential for T cell activation. *J Exp Med* 199: 369-379.
78. Timilsina, U., and R. Gaur. 2016. Modulation of apoptosis and viral latency - an axis to be well understood for successful cure of human immunodeficiency virus. *J Gen Virol* 97: 813-824.
79. Janardhan, A., T. Swigut, B. Hill, M. P. Myers, and J. Skowronski. 2004. HIV-1 Nef binds the DOCK2-ELMO1 complex to activate rac and inhibit lymphocyte chemotaxis. *PLoS Biol* 2: E6.
80. Simm, M., M. Shahabuddin, W. Chao, J. S. Allan, and D. J. Volsky. 1995. Aberrant Gag protein composition of a human immunodeficiency virus type 1 vif mutant produced in primary lymphocytes. *J Virol* 69: 4582-4586.
81. Ovod, V., A. Lagerstedt, A. Ranki, F. O. Gombert, R. Spohn, M. Tahtinen, G. Jung, and K. J. Krohn. 1992. Immunological variation and immunohistochemical localization of HIV-1 Nef demonstrated with monoclonal antibodies. *AIDS* 6: 25-34.

Footnotes

[1] Current address: Institut Cochin, INSERM U1016, CNRS UMR8104, Université Paris Descartes, Sorbonne Paris Cité, Paris, France.

[2] JB and AA contributed equally to this work as senior authors

[3] This work was supported by grants from the Agence Nationale de Recherche sur le SIDA et les Hepatitis Virales (ANRS, Grant AO 2013-02 CSS1 No 1339/14673), Sidaction (Grant VIH20160721001), the Institut Pasteur, INSERM, and the People Programme (Marie Sklodowska-Curie Actions) of the European Union's Seventh Framework Programme (Grant FP7/2007-2013, under the Research Executive Agency Grant agreement No 317057 HOMIN-ITN). The Photonic BioImaging UTechS microscopy facility at the Institut Pasteur is part of the France BioImaging infrastructure supported by Grant ANR-10-INSB-04-01, "Investments for the Future." Personnel's funding was as follows: IdR-I obtained predoctoral funding from the European Union Marie Curie Actions HOMIN-ITN (cited above), Fondation pour la Recherche Médicale and ANRS . IdR-I is a scholar in the Pasteur-Paris University International Doctoral program (PPU); EV-C received postdoctoral funding from Sidaction; JB received postdoctoral funding from ANRS, Roux-Institut Pasteur and Sidaction.

[4] IdRI and EVC design and performed experiments, analyzed data and contributed to manuscript writing. CC provided technical assistance. VdB provided expertise and critically read the manuscript. JB designed and performed experiments, analyzed data and critically read the manuscript. AA conceived the project, designed experiments, analyzed data and wrote the manuscript.

[5] Abbreviations used in this article: ANRS, Agence Nationale de Recherche sur le SIDA et les Hepatitis Virales; ERC, endosomal recycling compartment; FIP3, Rab11 family interacting protein-3; ICAReB, Institut Pasteur Clinical Investigation and Access to Biological Resources; IFT, intraflagellar transport protein; RT-qPCR, retrotranscription quantitative PCR; siRNA, small interfering RNA; WT, wild type.

Figure. Legends

Fig. 1: HIV-1-infected cells accumulate Lck and Rac1 in intracellular compartments in a Nef-dependent manner

Intracellular localization of endogenous Lck and Rac1 in primary human T cells (**A, B**) or Jurkat T cells (**C, D**). Cells were left uninfected (top panel), or infected with wild type HIV-1-WT (mid panel) or ΔNef (bottom panels) viruses. Three days post-infection, the subcellular localization of endogenous Lck and Rac1 was analyzed by immunofluorescence and confocal microscopy. Infected cells were identified by the expression of the HIV-1 capsid polypeptide of 24 kDa (p24). Bar, 3 μm in A, B and 5 μm in C, D.

A z-stack of 0.2 μm confocal optical sections was acquired for each cell. Three-dimensional (3D) confocal images were post-treated by deconvolution. A 0.4 μm-thick medial stack is shown. The pericentrosomal vesicular compartment is zoomed at the bottom right-hand corner in the middle column panels. Right column panels show density gradient fluorescent intensities in a color-code display of Lck or Rac1 localization. Images are representative of three experiments.

Figure. 2: HIV-1 Nef is sufficient to induce the accumulation of active Lck and Rac1 in the endosomal compartment

A: Intracellular localization of endogenous Lck and Nef in Jurkat T cells transfected with expression vectors encoding GFP (top) or Nef-GFP (bottom panel). Colocalization between endogenous Lck and GFP or Nef-GFP in the pericentrosomal compartment was assessed by the Pearsons's Correlation Coefficient (R) as described in Materials and Methods.

B: Intracellular localization of endogenous Lck phosphorylated on the activatory residue Tyr394 (pLck) and total Lck in Jurkat T cells expressing Nef-GFP. Colocalization between pLck and Lck in the pericentrosomal compartment was assessed as in A.

C: Intracellular localization of endogenous Rac1 and Nef in Jurkat T cells expressing GFP (top) or Nef-GFP (bottom panel). Colocalization between endogenous Rac1 and GFP or Nef-GFP in the pericentrosomal compartment was assessed as in A.

D, E: Intracellular localization of endogenous Lck and Rab11 (**D**), or Lck and the trans-Golgi network protein TGN46 (**E**) in Jurkat T cells expressing Nef-GFP. Colocalization between endogenous Lck and Rab11 or Lck and TGN46 in the pericentrosomal compartment was assessed as in A.

A-E: A z-stack of 0.2 μm confocal optical sections was acquired for each cell. 3D confocal images were post-treated by deconvolution. A 0.4-μm-thick medial stack is shown. Bottom right corner of each image corresponds to a zoomed image of the pericentrosomal vesicular compartment of each cell. Bar, 5 μm. Images are representative of three experiments.

Figure. 3: The Nef-induced Lck endosomal compartment gathers signaling competent phosphorylated forms of TCRζ, ZAP70, SLP76 and Vav1, but not LAT

A-E: Jurkat T cells expressing GFP (top) or Nef-GFP (bottom), in which the localization of endogenous phosphorylated signaling proteins was assessed by immunofluorescence, using antibodies directed to specific phosphotyrosine (pTyr) residues. A z-stack of 0.2 μm-confocal optical sections was acquired for each cell. 3D confocal images were post-treated by deconvolution. A 0.4-μm-thick medial stack is shown. Bottom right corner of each image corresponds to a zoomed image of the pericentrosomal vesicular compartment of each cell. Analysis of colocalization between endogenous Lck and pTyr142-TCRζ (**A**), pTyr319-ZAP70 (**B**), pTyr191-LAT (**C**), pTyr128-SLP76 (**D**) and pTyr174-Vav1 (**E**) in the pericentrosomal compartment was assessed by the Pearsons's Correlation Coefficient (R). Bar, 5 μm. Images are representative of three experiments.

Right column plots show cell population analyses of R values of the different phospho-proteins. Each dot corresponds to a different cell. Horizontal bars represent the mean ± SEM, Mann-Whitney *U*-test was used. ****, $p<0.0001$; ***, $p<0.001$; **, $p<0.01$; *, $p<0.05$; non-significant (ns), $p \geq 0.05$.

Figure. 4: Recruitment of phosphorylated Zap70 is dependent on Nef's ability to generate the Lck endosomal compartment

A: Intracellular localization of endogenous Lck and phospho-proteins in Jurkat T cells expressing GFP or Nef-GFP. A z-stack of 1 μm confocal optical sections was acquired for each cell. Localization of endogenous proteins was assessed by immunofluorescence as in 3A-E. Plots represent the % fluorescence intensity of phospho-proteins in the area corresponding to the Lck compartment divided by the fluorescence intensity of phospho-protein in the whole cell area, as described in Methods. Each dot represents one cell. Horizontal bars represent the mean ± SEM. Mann-Whitney *U*-test was used. ****, $p<0.0001$; ***, $p<0.001$; **, $p<0.01$; *, $p<0.05$; non-significant (ns), $p \geq 0.05$.

B: Jurkat T cells expressing Nef PXXP/AXXA-GFP (top) or GFP (bottom), in which the localization of endogenous Lck and pTyr319-ZAP70 proteins was assessed by immunofluorescence and confocal microscopy. A z-stack of 0.2 μm-confocal optical sections was acquired for each cell. 3D confocal images were post-treated by deconvolution. A 0.4-μm-thick medial stack is shown. Bottom right corner of each image corresponds to a zoomed image of the pericentrosomal vesicular compartment of each cell. Bar, 5 μm. Images are representative of three experiments.

C: Cell population analysis of colocalization between Lck and pZAP70 in GFP and Nef PXXP/AXXA-GFP cells in the pericentrosomal compartment was assessed as in 3A-E. Each dot represents one cell. Horizontal bars represent the mean ± SEM. Mann-Whitney *U*-test was used. Non-significant (ns), $p \geq 0.05$.

D: Fluorescence intensity levels of pZAP70 in unstimulated Jurkat cells expressing GFP, Nef-GFP and Nef PXXP/AXXA-GFP cells were analyzed by flow cytometry. Horizontal bars represent the mean ± SEM. Data are the mean of three independent biological experiments, with 2 replicates per experiment. T student test was used. ****, $p<0.0001$; **, $p<0.01$; *, $p<0.05$.

Figure. 5: Nef induces the accumulation of CD28 in a pericentrosomal compartment where it partially co-localizes with Rac1, but not with phosphorylated Vav1

A: Intracellular localization of endogenous CD28 in Jurkat T cells expressing GFP (top panels) or Nef-GFP (bottom panels) were analyzed by immunofluorescence and confocal microscopy. A z-stack of 0.2-μm-confocal optical sections was acquired for each cell. 3D confocal images were post-treated by deconvolution. A 0.4-μm-thick medial stack is shown. Bottom right corner of each image corresponds to a zoomed image of the pericentrosomal vesicular compartment of each cell. Bar, 5 μm. Images representative of three experiments.

B: Cell population analysis of colocalization between Nef-GFP and CD28 in the pericentrosomal compartment was assessed as in Fig. 3. Each dot represents one cell. Horizontal bars represent the mean ± SEM.

C-F: Intracellular localization of endogenous pTyr174-Vav1 and CD28 (**C-D**) and Rac1 and CD28 (**E-F**) in Nef-GFP cells was analyzed by immunofluorescence and confocal microscopy. A z-stack of 0.2-μm-confocal optical sections was acquired for each cell. 3D confocal images were post-treated by deconvolution. A 0.4-μm-thick medial stack is shown.

Bottom right corner of each image corresponds to a zoomed image of the pericentrosomal vesicular compartment of each cell. Bar, 5 μm. Images representative of three experiments.

Cell population analysis of colocalization between pTyr-174Vav1 and CD28 (**D**) and Rac1 and CD28 (**F**) in the pericentrosomal compartment was assessed as in Fig. 3. Each dot represents one cell. Horizontal bars represent the mean ± SEM.

Figure. 6: Effect of HIV-1 Nef on gene expression

A-C: Jurkat T cells were left uninfected (Ctrl) or infected with HIV-1 WT or ΔNef viruses. Two days post-infection, non-stimulated cells were lysed and mRNA expression levels of the early activation genes *JUN*, *FOS* and *MYC* (**A**), of the NFκB target genes, *TNFAPI3*, and *NFKBIA* (**B**), and of the late activation genes, *IL2*, *IFNG* (IFNγ) and *IL2RA (CD25)* (**C**) were assessed by RT-qPCR and normalized to the *B2M* housekeeping gene. Data are the mean ± SEM values (n=4) of a representative experiment out of three independent experiments performed. T student test was used ****, $p < 0.0001$; ***, $p < 0.001$; **, $p < 0.01$; *, $p < 0.05$; non-significant (ns), $p \geq 0.05$

D: Jurkat T cells were transfected with GFP or Nef-GFP expression vectors. 24h later, GFP positive cells were sorted, lysed and the mRNA expression levels of *JUN*, *FOS*, *MYC*, *TNFAPI3* and *NFKBIA* were assessed by RT-qPCR and normalized to the *B2M* housekeeping gene. Data are the mean of seven independent biological experiments, with four replicates per experiment. Plots represent mean ± SEM values (n=28). Mann-Whitney *U*-test was used. ***, $p < 0.001$; *, $p < 0.05$; non-significant (ns), $p \geq 0.05$.

Figure. 7: FIP3 silencing disaggregates the Nef-induced Lck compartment

A-C: Jurkat T cells were co-transfected with control (siCtrl) or FIP3 (siFIP3) siRNA oligonucleotides and with GFP or Nef-GFP expression vectors as described in Methods. Nef-GFP, endogenous Lck and pTyr319-ZAP70 subcellular localization was analyzed by immunofluorescence and confocal microscopy. A z-stack of 0.2 μm confocal optical sections was acquired for each cell. 3D confocal images were post-treated by deconvolution.

A: a 0.4-μm-thick medial stack is shown. Bar 5 μm. Images representative of three experiments.

B: Densitometry profiles of pTyr319-ZAP70 across the largest cytoplasmic area, including plasma membrane and the pericentrosomal Lck compartment, were obtained as described in Methods. Four representative cells are shown out of twenty analyzed.

C: Western Blot analysis of lysates from Jurkat T cells transfected as described in A-C. Blot shows the band corresponding to FIP3 and β-Tubulin proteins.

Figure. 8: FIP3 silencing counteracts HIV-1 effects on T cell gene expression

A-D: Jurkat T cells were transfected with siCtrl or siFIP3 oligonucleotides. 36 h later, cells were left uninfected (Ctrl) or infected with HIV-1 WT or ΔNef viruses for 36 h, as described in Materials and Methods.

A: Western Blot analysis of lysates from control and infected Jurkat T cells. Bands corresponding to FIP3, and Nef and p24 viral proteins and GAPDH as internal control are depicted. Note that FIP3 has two isoforms of slightly different electrophoretic mobility (double arrow head). SiFIP3-1 preferentially silenced, though partially, the one of higher molecular mass, whereas siFIP3-2 silenced both more efficiently.

B-C: Infected cells were lysed and mRNA levels of *JUN*, *FOS* (**B**), *NFKBIA*, *IFNG* and *IL2* (**C**) were assessed by RT-qPCR and normalized to the *B2M* housekeeping gene mRNA. Data show the mean ± SEM values with n=4 from a representative experiment out of three independent experiments. Two-Way ANOVA was used. For clarity only statistics between the WT and ΔNef conditions are shown. ****, $p < 0.0001$; **, $p < 0.01$; non-significant (ns), $p \geq 0.05$

D: KC57-FITC labelled antibody was used to analyze infection levels (HIV-1 proteins 55, 39, 33 & 24 kDa of core antigen) by flow cytometry.

Figure. 9: Nef expression sequesters Rac1 and inhibits Rac-1-dependent T cell spreading induced by FIP3 silencing

A, B: Jurkat T cells (**A**) or CD4 primary T cells (**B**) were transfected with GFP (top) or Nef-GFP (bottom) expression vectors and the intracellular localization of endogenous Rac1 was analyzed by immunofluorescence and confocal microscopy. A z-stack of 0.2-μm-confocal optical sections was acquired for each cell. 3D confocal images were post-treated by deconvolution. A 0.4-μm-thick medial stack is shown. Bottom right corner of each image

corresponds to a zoomed image of the pericentrosomal vesicular compartment of each cell. Bar 5 μm (**A**) and 3 μm (**B**). Images representative of three experiments.

C: Cell population analysis of colocalization between endogenous Rac1 and Nef-GFP in the Nef-induced compartment assessed by the Pearsons's Correlation Coefficient (R). Each dot represents one cell. Horizontal bars represent the mean ± SEM.

D-F: Jurkat T cells were co-transfected with control (siCtrl) or FIP3 (siFIP3) siRNA oligonucleotides and GFP or Nef-GFP expression vectors, as described in Methods. Subcellular localization of Nef-GFP, and endogenous Rac1 was analyzed by immunofluorescence and confocal microscopy. A z-stack of 0.2 μm confocal optical sections was acquired for each cell. 3D confocal images were post-treated by deconvolution.

D: A 0.4-μm-thick medial stack is shown. Bottom right corner of each image corresponds to a zoomed image of the pericentrosomal vesicular compartment of each cell. Representative of three experiments. Bar 5 μm.

E: Densitometry profiles across cells including plasma membrane and the pericentrosomal Nef and Rac1 compartment were obtained as described in Methods. Four representative cells are shown out of twenty analyzed.

F: Cell population analysis of colocalization between Nef-GFP and Rac1 in the Nef-induced compartment was assessed as in C. Each dot represents one cell. Horizontal bars represent the mean ± SEM. Mann-Whitney *U*-test was used. Non-significant (ns), $p \geq 0.05$.

G: Jurkat T cells were co-transfected with control (siCtrl) or FIP3 (siFIP3) siRNA oligonucleotides and GFP or Nef-GFP expression vectors, as described in Methods. Cells were allowed to spread on poly-lysine-coated coverslips for 2, 5 or 15 min, and F-actin was stained using a fluorescent-labelled Phalloidin. Cells were analyzed by confocal microscopy. Cell contact surface was measured using ImageJ, as described in Methods. A z-stack of 0.2 μm confocal optical sections was acquired for each cell. 3D confocal images were post-treated by deconvolution. A 0.4-μm thick stack at the contact surface is shown. Bar 3 μm. Images representative of three experiments

H: Cell population analysis dot plots displaying spreading area values at 5 and 15 min. Each dot represents one cell. Horizontal bars represent the mean ± SEM. Mann-Whitney *U*-test was used. ****, $p < 0.0001$; non-significant (ns), $p \geq 0.05$.

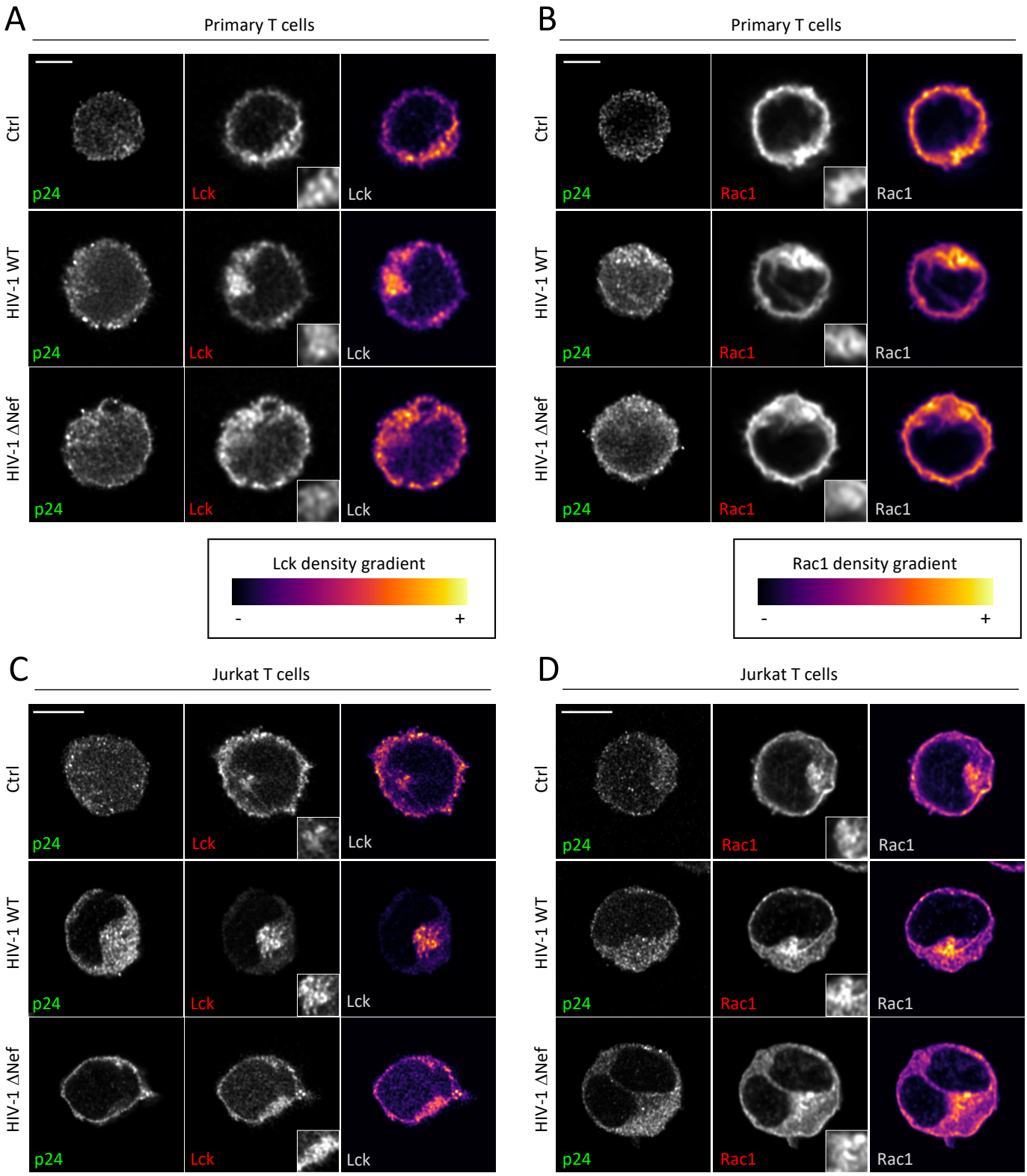
A
Primary T cells
Ctrl
HIV-1 WT
HIV-1 ΔNef
p24
Lck
Lck density gradient
-
+
B
Primary T cells
Rac1
Rac1 density gradient
C
Jurkat T cells
D
Jurkat T cells

Figure 1

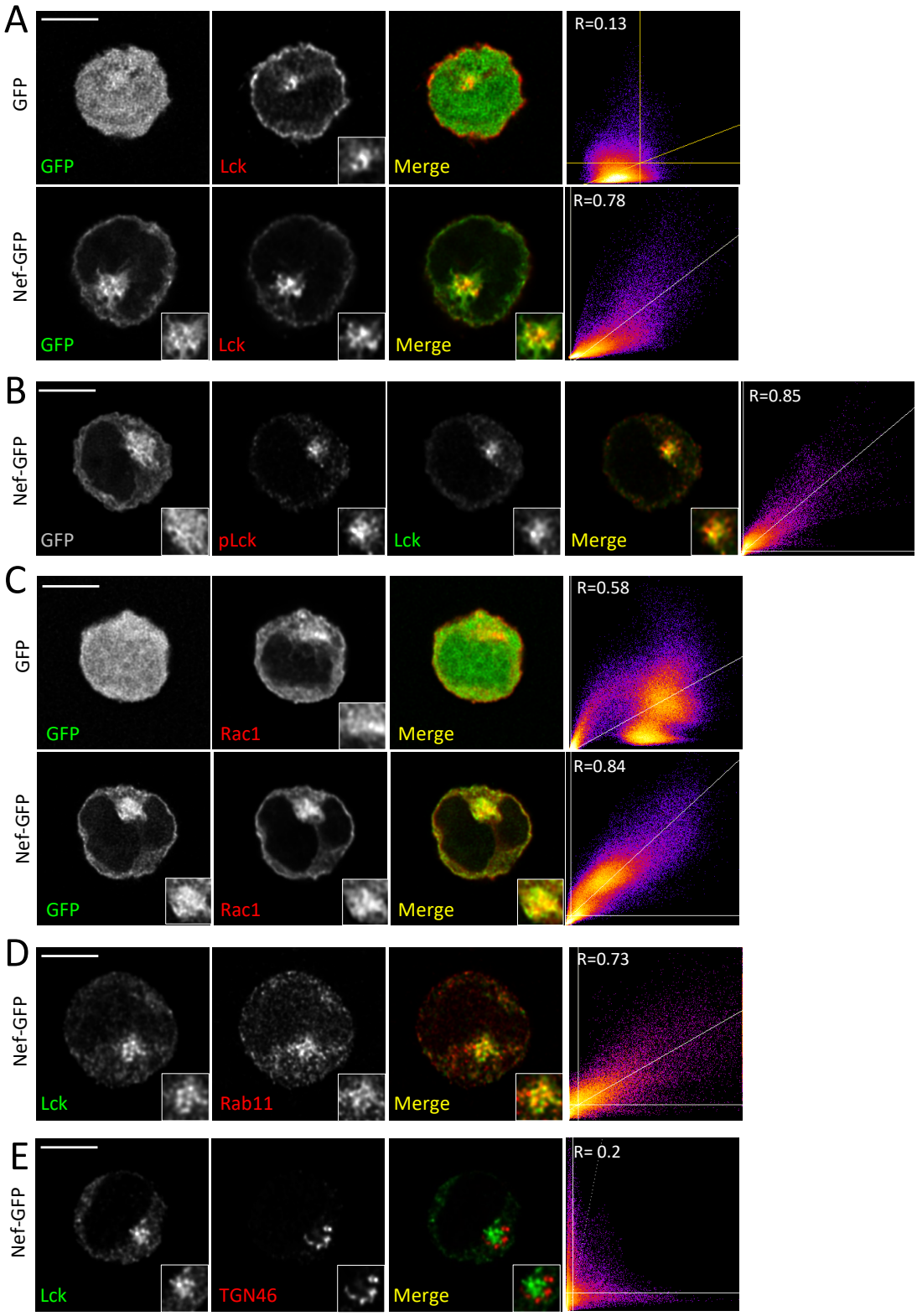
A
GFP
GFP
Lck
Merge
R=0.13
Nef-GFP
GFP
Lck
Merge
R=0.78
B
Nef-GFP
GFP
pLck
Lck
Merge
R=0.85
C
GFP
GFP
Rac1
Merge
R=0.58
Nef-GFP
GFP
Rac1
Merge
R=0.84
D
Nef-GFP
Lck
Rab11
Merge
R=0.73
E
Nef-GFP
Lck
TGN46
Merge
R= 0.2

Figure 2

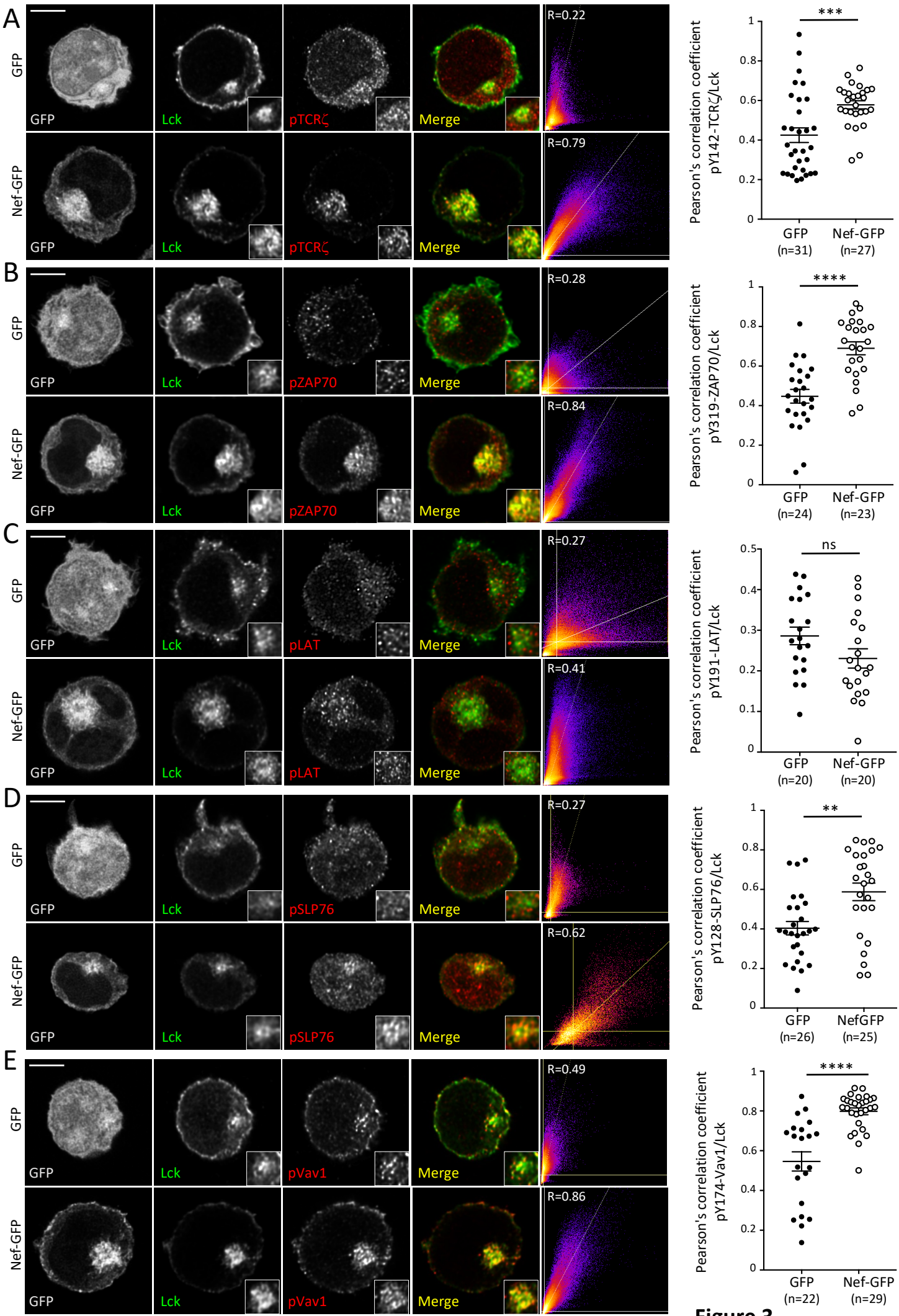
A
GFP
Nef-GFP
GFP
Lck
pTCRζ
Merge
R=0.22
R=0.79
Pearson's correlation coefficient pY142-TCRζ/Lck
***
GFP (n=31)
Nef-GFP (n=27)
B
pZAP70
R=0.28
R=0.84
Pearson's correlation coefficient pY319-ZAP70/Lck
****
GFP (n=24)
Nef-GFP (n=23)
C
pLAT
R=0.27
R=0.41
Pearson's correlation coefficient pY191-LAT/Lck
ns
GFP (n=20)
Nef-GFP (n=20)
D
pSLP76
R=0.27
R=0.62
Pearson's correlation coefficient pY128-SLP76/Lck
**
GFP (n=26)
NefGFP (n=25)
E
pVav1
R=0.49
R=0.86
Pearson's correlation coefficient pY174-Vav1/Lck
****
GFP (n=22)
Nef-GFP (n=29)

Figure 3

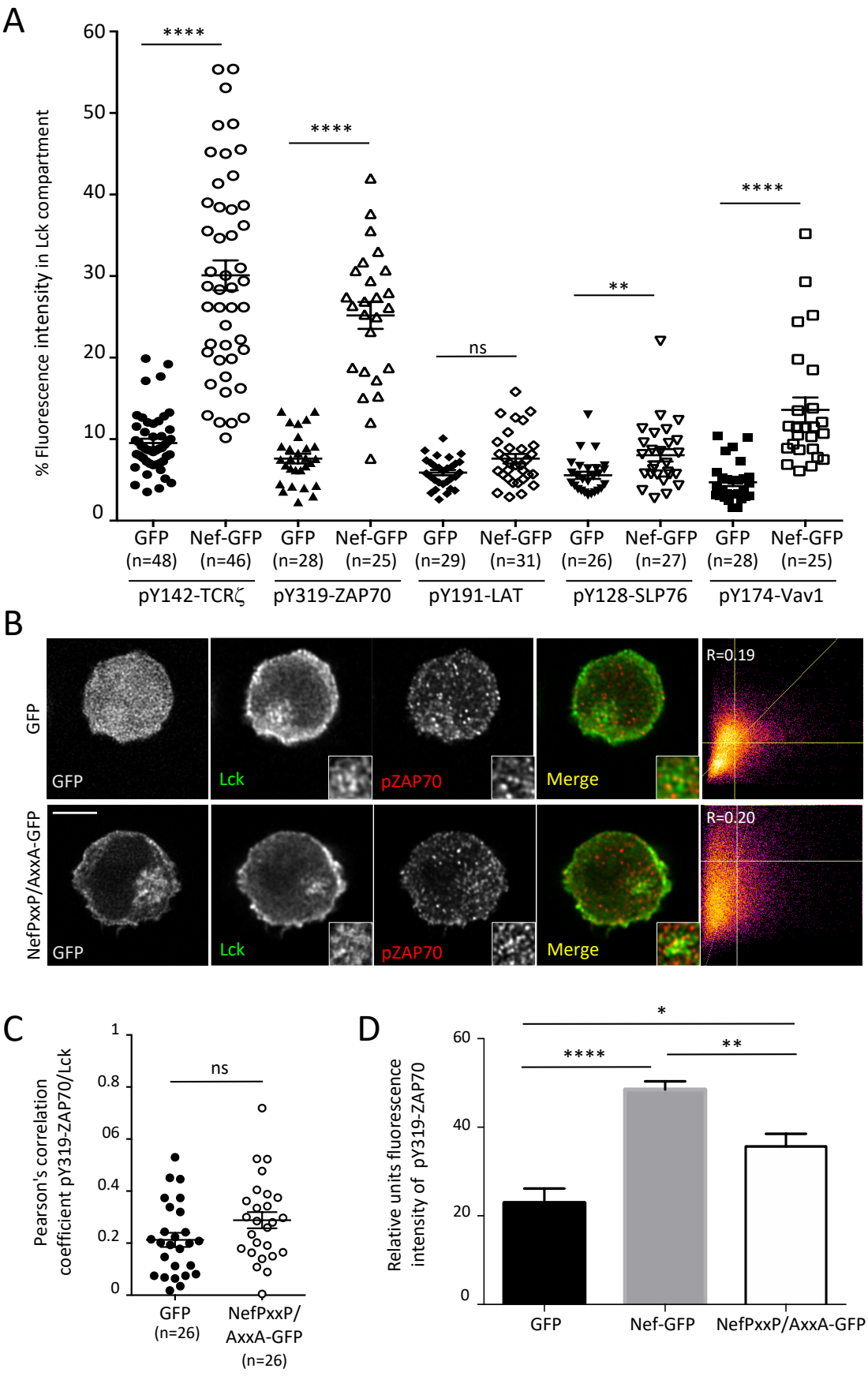
A
% Fluorescence intensity in Lck compartment
60
50
40
30
20
10
0
****
****
ns
**
****
GFP (n=48)
Nef-GFP (n=46)
GFP (n=28)
Nef-GFP (n=25)
GFP (n=29)
Nef-GFP (n=31)
GFP (n=26)
Nef-GFP (n=27)
GFP (n=28)
Nef-GFP (n=25)
pY142-TCRζ
pY319-ZAP70
pY191-LAT
pY128-SLP76
pY174-Vav1
B
GFP
NefPxxP/AxxA-GFP
GFP
Lck
pZAP70
Merge
R=0.19
R=0.20
C
Pearson's correlation coefficient pY319-ZAP70/Lck
1
0.8
06
0.4
0.2
0
ns
GFP (n=26)
NefPxxP/ AxxA-GFP (n=26)
D
Relative units fluorescence intensity of pY319-ZAP70
60
40
20
0
*
****
**
GFP
Nef-GFP
NefPxxP/AxxA-GFP

Figure 4

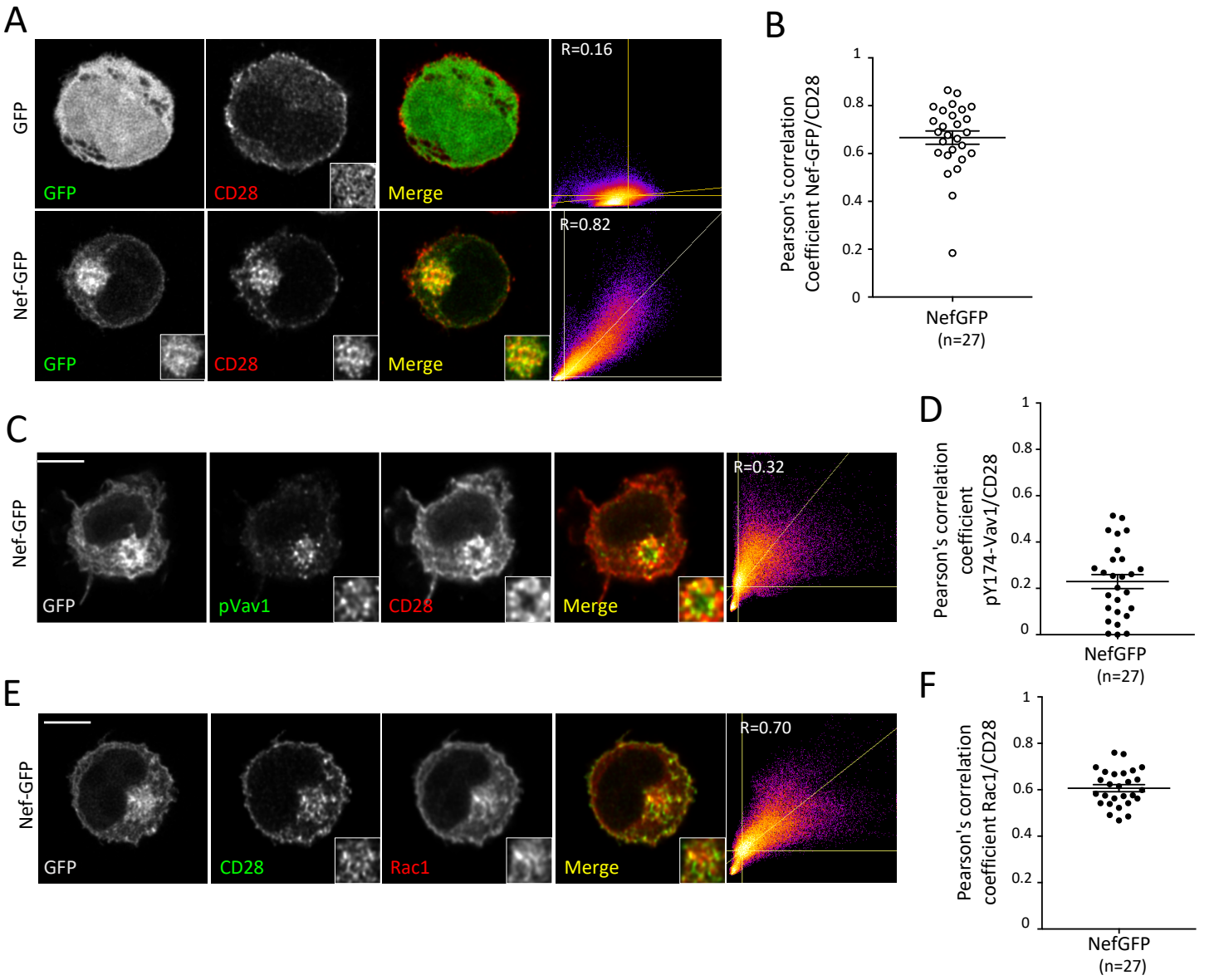
A
GFP
Nef-GFP
GFP
CD28
Merge
R=0.16
R=0.82
B
Pearson's correlation
Coefficient Nef-GFP/CD28
1
0.8
0.6
0.4
0.2
0
NefGFP
(n=27)
C
Nef-GFP
GFP
pVav1
CD28
Merge
R=0.32
D
Pearson's correlation
coefficient
pY174-Vav1/CD28
1
0.8
0.6
0.4
0.2
0
NefGFP
(n=27)
E
Nef-GFP
GFP
CD28
Rac1
Merge
R=0.70
F
Pearson's correlation
coefficient Rac1/CD28
1
0.8
0.6
0.4
0.2
0
NefGFP
(n=27)

Figure 5

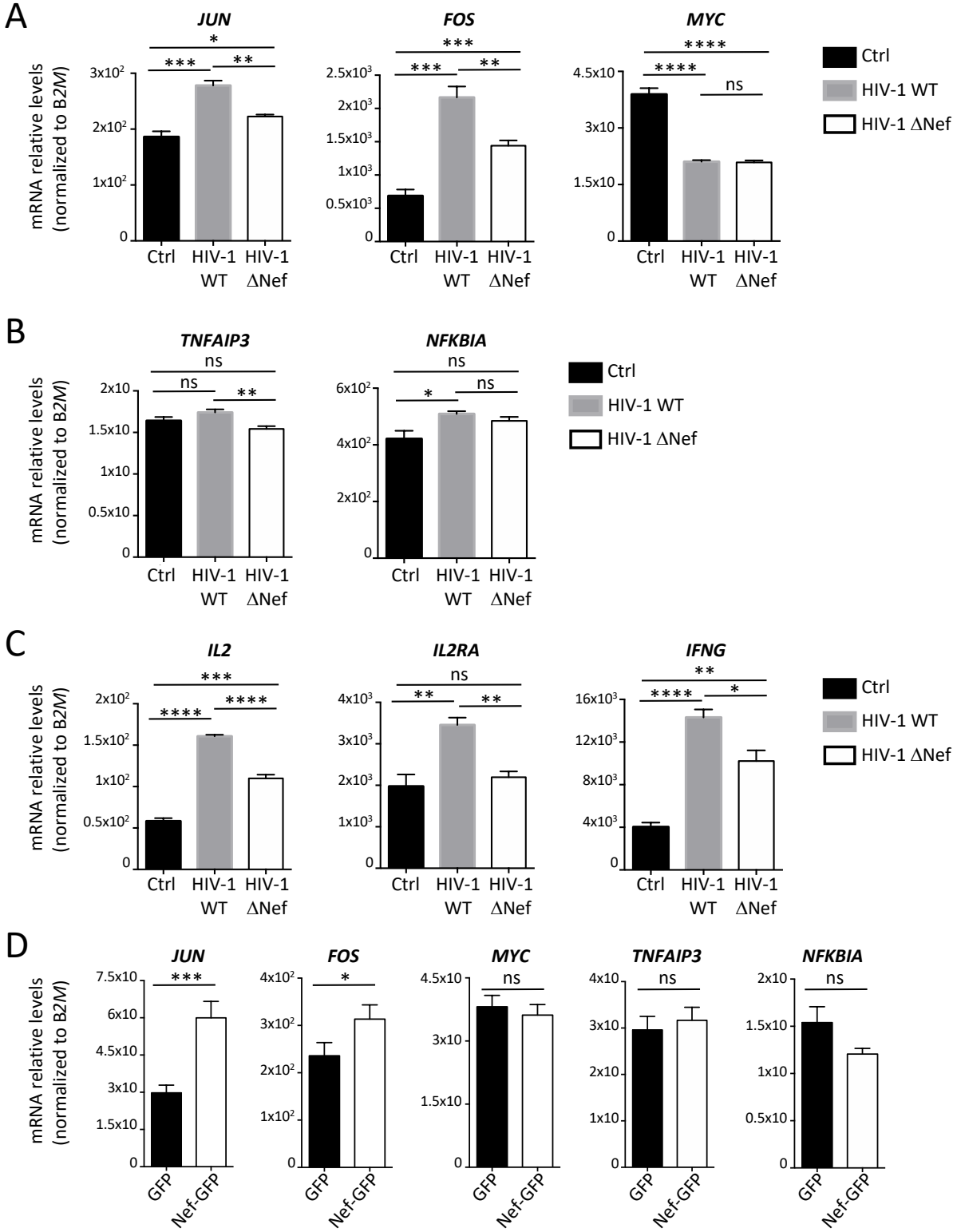
A
JUN
FOS
MYC
mRNA relative levels (normalized to B2M)
Ctrl
HIV-1 WT
HIV-1 ΔNef
B
TNFAIP3
NFKBIA
C
IL2
IL2RA
IFNG
D
GFP
Nef-GFP
ns

Figure 6

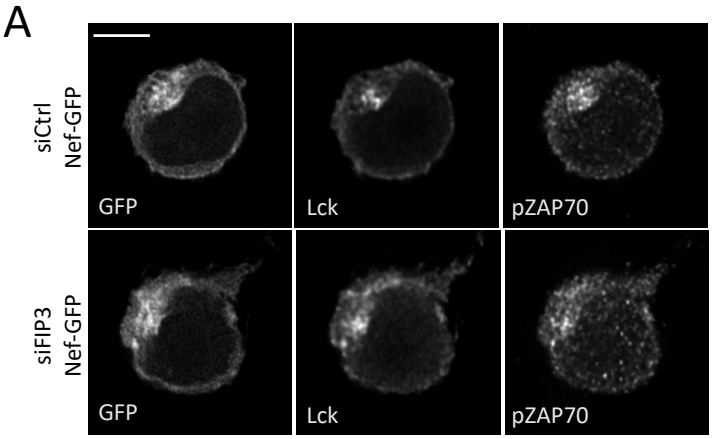
A
siCtrl Nef-GFP
siFIP3 Nef-GFP
GFP
Lck
pZAP70
GFP
Lck
pZAP70

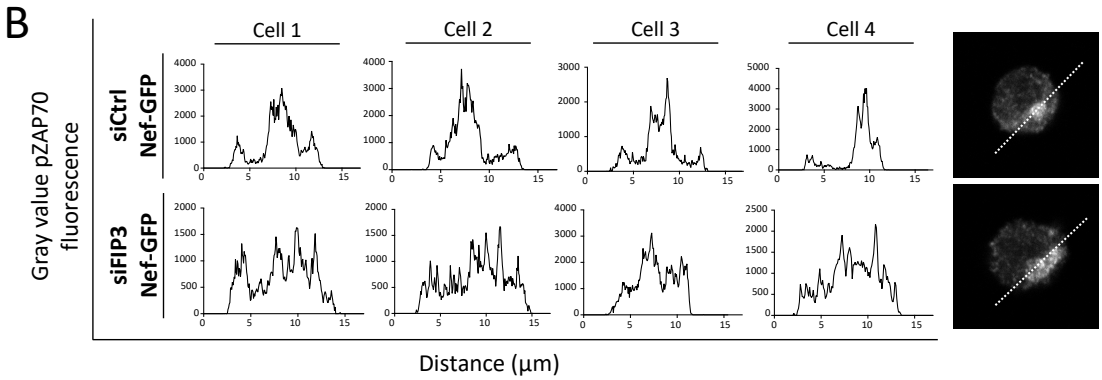
B
Gray value pZAP70 fluorescence
Cell 1
Cell 2
Cell 3
Cell 4
siCtrl Nef-GFP
siFIP3 Nef-GFP
Distance (µm)

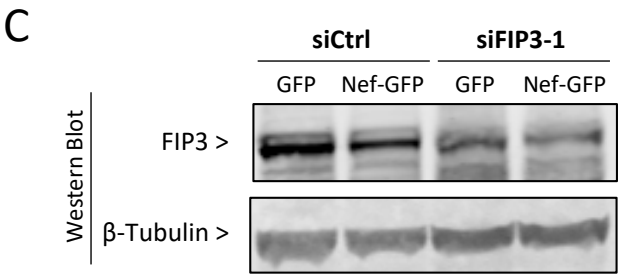
C
siCtrl
siFIP3-1
GFP
Nef-GFP
GFP
Nef-GFP
Western Blot
FIP3 >
β-Tubulin >

Figure 7

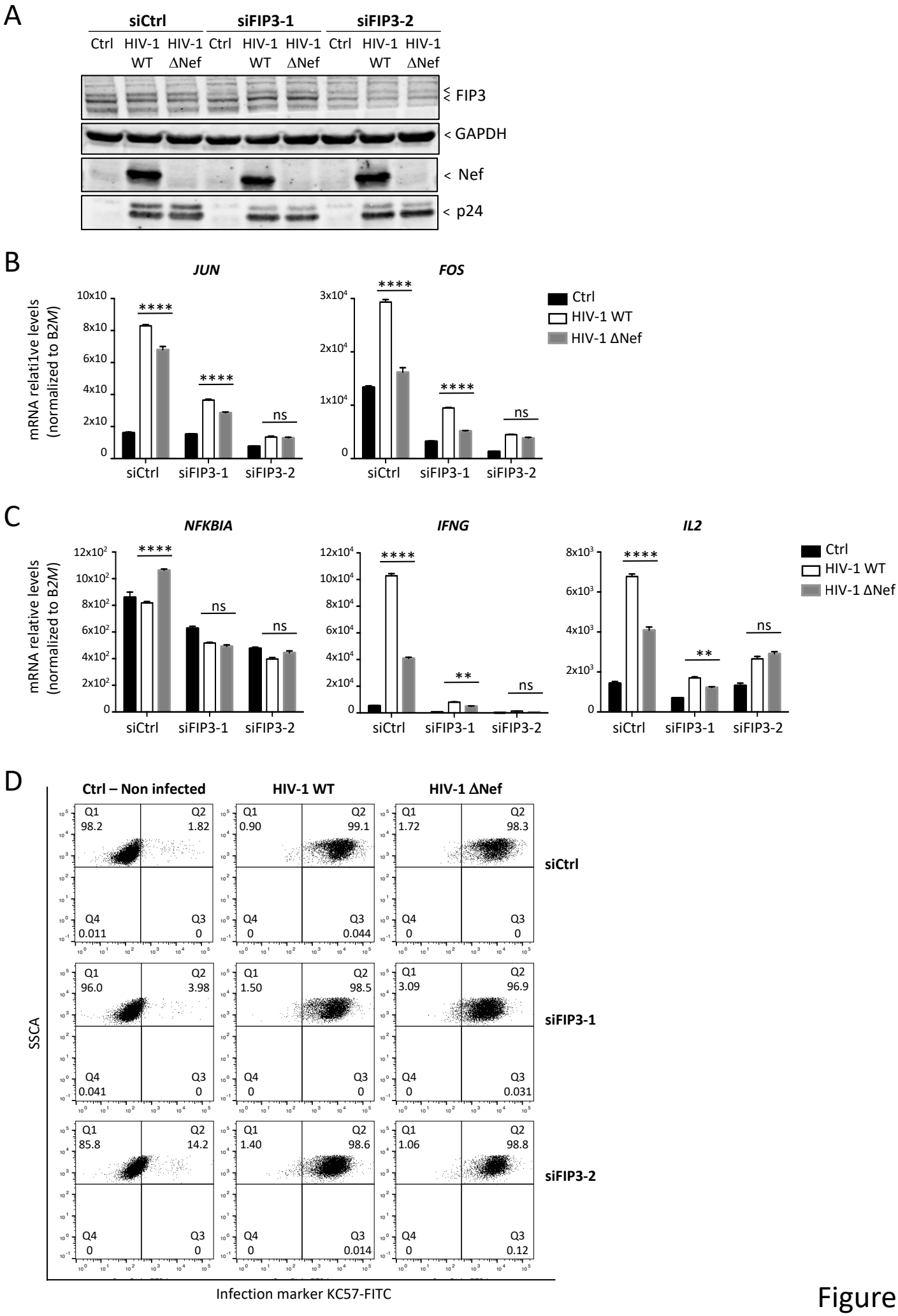
A
siCtrl
siFIP3-1
siFIP3-2
Ctrl
HIV-1 WT
HIV-1 ΔNef
FIP3
GAPDH
Nef
p24
B
JUN
FOS
mRNA relati1ve levels (normalized to B2M)
Ctrl
HIV-1 WT
HIV-1 ΔNef
****
ns
siCtrl
siFIP3-1
siFIP3-2
C
NFKBIA
IFNG
IL2
mRNA relative levels (normalized to B2M)
**
D
Ctrl – Non infected
HIV-1 WT
HIV-1 ΔNef
Q1 98.2
Q2 1.82
Q4 0.011
Q3 0
Q1 0.90
Q2 99.1
Q4 0
Q3 0.044
Q1 1.72
Q2 98.3
Q4 0
Q3 0
Q1 96.0
Q2 3.98
Q4 0.041
Q3 0
Q1 1.50
Q2 98.5
Q4 0
Q3 0
Q1 3.09
Q2 96.9
Q4 0
Q3 0.031
Q1 85.8
Q2 14.2
Q4 0
Q3 0
Q1 1.40
Q2 98.6
Q4 0
Q3 0.014
Q1 1.06
Q2 98.8
Q4 0
Q3 0.12
SSCA
Infection marker KC57-FITC

Figure 8

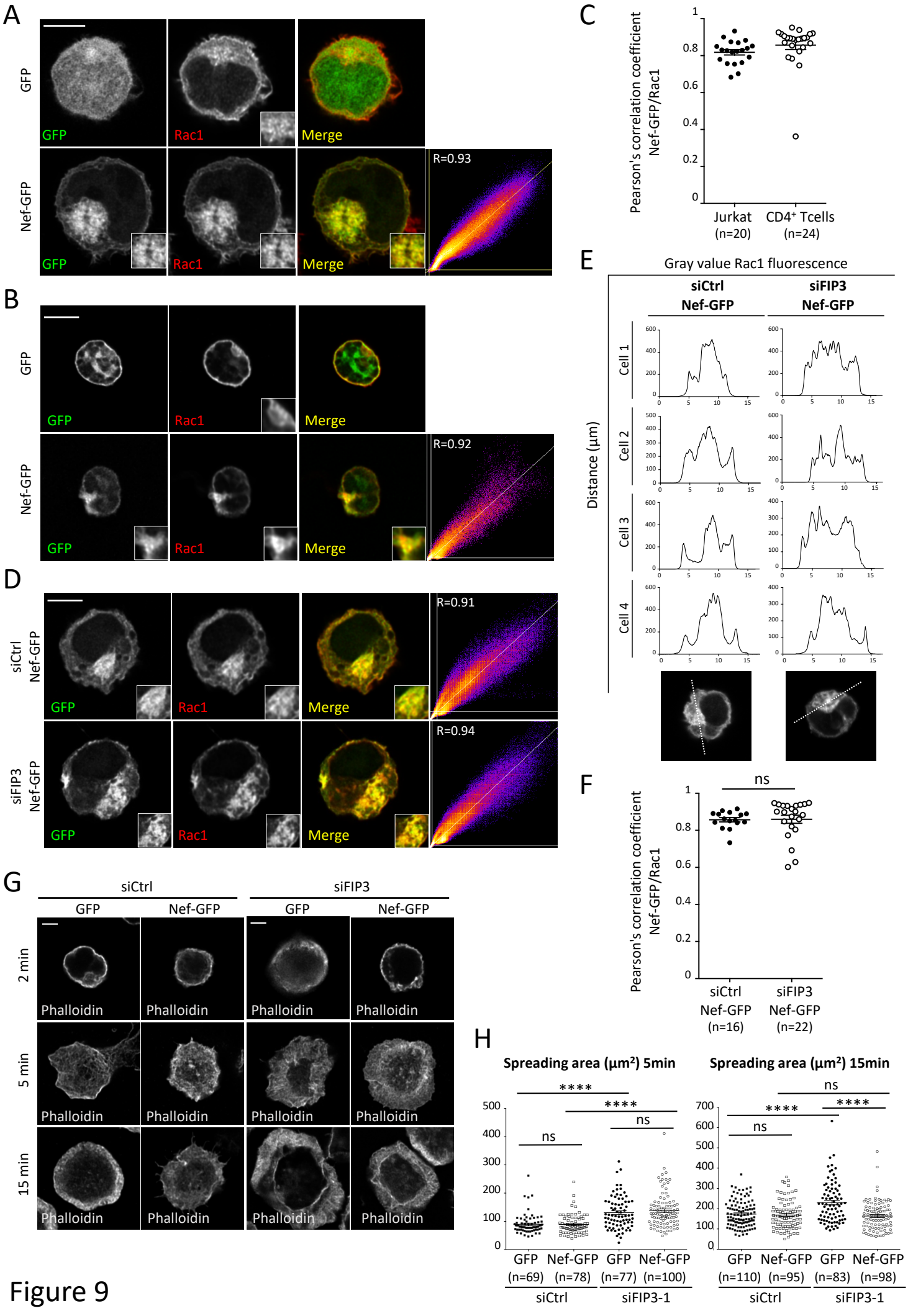
A
GFP
Nef-GFP
GFP
Rac1
Merge
R=0.93
B
R=0.92
C
Pearson's correlation coefficient
Nef-GFP/Rac1
Jurkat
(n=20)
CD4+ Tcells
(n=24)
D
siCtrl
Nef-GFP
siFIP3
Nef-GFP
R=0.91
R=0.94
E
Gray value Rac1 fluorescence
siCtrl
Nef-GFP
siFIP3
Nef-GFP
Cell 1
Cell 2
Cell 3
Cell 4
Distance (µm)
F
ns
siCtrl
Nef-GFP
(n=16)
siFIP3
Nef-GFP
(n=22)
G
siCtrl
siFIP3
GFP
Nef-GFP
2 min
5 min
15 min
Phalloidin
H
Spreading area (µm²) 5min
Spreading area (µm²) 15min
****
ns
GFP
(n=69)
Nef-GFP
(n=78)
GFP
(n=77)
Nef-GFP
(n=100)
siCtrl
siFIP3-1
GFP
(n=110)
Nef-GFP
(n=95)
GFP
(n=83)
Nef-GFP
(n=98)

Figure 9

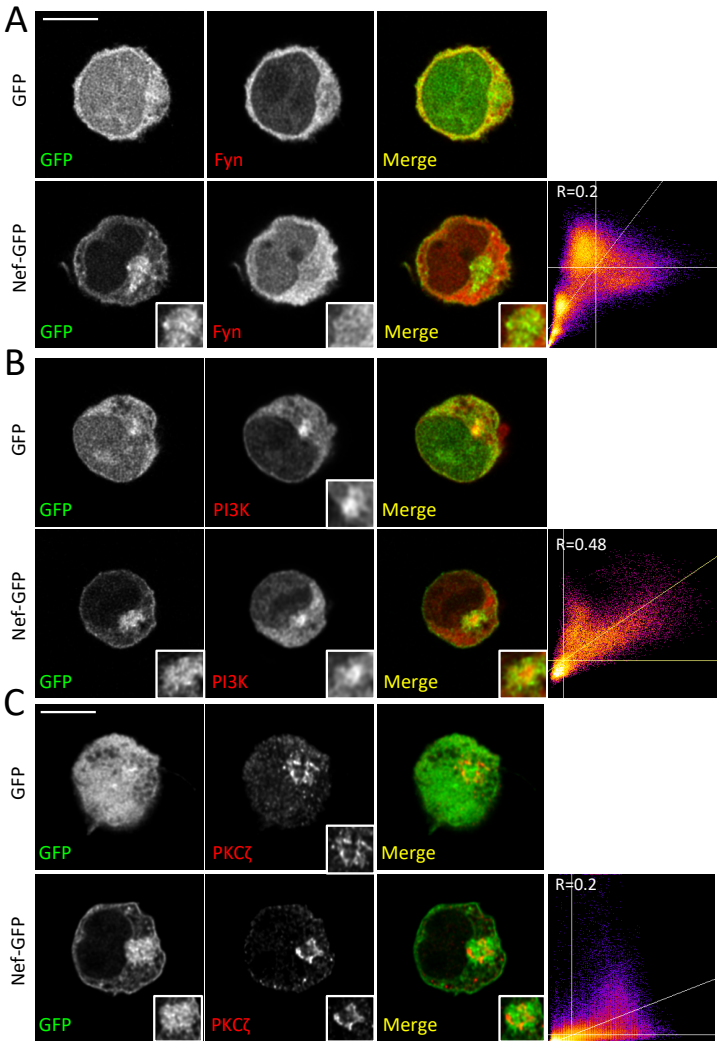

D

Protein	Localization
CD28, Lck, pY394-Lck, pY128-SLP76, pY142-TCRζ, pY319-ZAP70, pY174-Vav1, Rac1	Re-localized in the Nef-induced compartment
AKT, LAT, NEMO, pY783-PLCγ1, Vav1, ZAP70	Partially re-localized in the Nef-induced compartment
Bcl10, CARMA, Fyn, mTOR, NF-kappaB (p105 and p65 subunits), PI3K, PKCθ, PKCζ, pT202/Y204-Erk1/2, pY185-JNK, pY191-LAT, pT538-PKCθ, Rab11, TGN46	Non re-localized in the Nef-induced compartment

Supplementary Figure 1: Nef does not induce the relocalization of signaling effectors downstream of Lck, TCRζ, ZAP70 and Vav1

A-D: Localization of endogenous signaling proteins of the TCR and CD28 signaling pathways were analyzed in Jurkat T cells expressing GFP (top) or Nef-GFP (bottom) by immunofluorescence, using antibodies directed to the proteins or to specific phosphorylated amino acid residues (tyrosine or threonine) characterizing their signaling competent state.

A-C: Localization of endogenous Fyn (A), PI3K (B) and PKCζ (C) by immunofluorescence and confocal microscopy, here shown as examples of the numerous proteins analyzed and summarized in D. A z-stack of 0.2 µm-confocal optical sections was acquired for each cell. 3D confocal images were post-treated by deconvolution. A 0.4-µm-thick medial stack is shown. Bottom right corner of each image corresponds to a zoomed image of the pericentrosomal vesicular compartment of each cell. Analysis of colocalization between Nef-GFP and endogenous proteins was assessed by the Pearsons's Correlation Coefficient (R). Bar, 5 µm.

D: List of the endogenous signaling proteins whose intracellular localization was analyzed during this study. Protein distributions assessed by visual observation of two observers were classified in 3 groups: re-localized in the Nef or the Nef-induced Lck pericentrosomal compartment (see figures in the main text), partially re-localized and no re-localized in those compartments. Localization of the proteins or their phosphorylated residues is depicted.

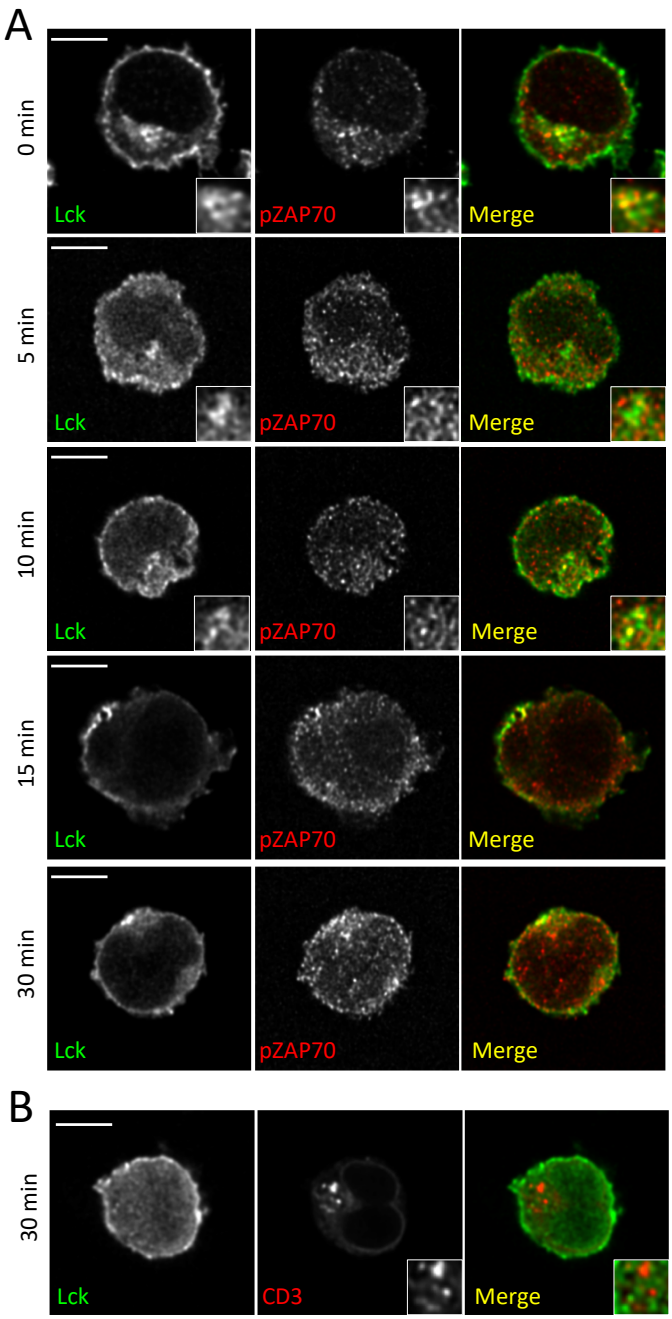

Supplementary Figure 2: CD3-CD28 stimulation does not mimic the Nef-induced Lck endosomal signaling compartment

A-B: Jurkat T cells transfected with GFP expression vector**.** Localization of endogenous Lck and phosphoTyr319-ZAP70 **(A)** or the internalized CD3 **(B)** after the indicated times of CD3-CD28 stimulation was assessed by immunofluorescence.

A z-stack of 0.2 µm-confocal optical sections was acquired for each cell. 3D confocal images were post-treated by deconvolution. A 0.4-µm-thick medial stack is shown. Bottom right corner images correspond to a zoomed image of the pericentrosomal vesicular compartment of each cell. Bar, 5 µm. Images representative of three experiments.

Primary antibodies/reagents - Specificity - Clone	Host-Isotype	Source	Dilution
Used in immunofluorescence			
AKT (pan) (40D4)	mouse IgG1	Cell Signaling	1:50
BCL10 (A48)	mouse IgG1	OriGene	7.3 μg/ml (1:100)
CARMA1 (CARD11)	rabbit	Abcam	33.3 μg/ml (1:30)
CD28 (B-T3)	mouse IgG2a	Abcam	10 μg/ml (1:100)
F-actin (Phalloidin - Texas Red)	Phallotoxin	Invitrogen	1:100
Fyn (FYN-01)	mouse IgG2b	Abcam	10 μg/ml (1:100)
HIV-1 p24 antiserum (Lot 060880)	rabbit	NIH AIDS Reagent Program	1:120
LAT	rabbit	Upstate Biotechnology	3.3 μg/ml (1:300)
Lck (3A5)	mouse IgG2b	Santa Cruz Biotechnology	2 μg/ml (1:100)
mTORC (7C10)	rabbit	Cell Signaling	1:400
NEMO	rabbit	Gift from Robert Weil	1:500
NF-κB (p105/50)	rabbit	Gift from Robert Weil	1:100
NF-κB (p65) (C-20)	rabbit	Santa Cruz Biotechnology	4 μg/ml (1:50)
Phospho-CD3ζ(Y142) (k25-407.69)	mouse IgG2a	Becton Dickinson	5 μg/ml (1:100)
Phospho-Erk1/2(T202/Y204) (D13.14.4E)	rabbit	Cell Signaling	1:200
Phospho-LAT(Y191)	rabbit	Cell Signaling	1:100
Phospho-PLCγ(Y783)	rabbit	Cell Signaling	1:100
Phospho-PKCθ(T538)	rabbit	Cell Signaling	1:100
Phospho-SAPK/JNK(T183/Y185) (G9)	mouse IgG1	Cell Signaling	1:400
Phospho-SLP76(Y128) (J141-668.36.58)	mouse IgG1	Becton Dickinson	2.5 μg/ml (1:200)
Phospho-Src family(Y416) (used to detect pY394-Lck)	rabbit	Cell Signaling	1:100
Phospho-ZAP70(Y319)/SYK(Y352) (65E4)	rabbit	Cell Signaling	1:100
Phospho-Vav1(Y174)	rabbit	Abcam	2.26 μg/ml (1:100)
PI3K (p85)	rabbit	Gift from S. Etienne-Manneville	1:100
PKCθ	mouse IgG2a	Becton Dickinson	2.5 μg/ml (1:100)
PKCζ (C-20)	rabbit	Santa Cruz Biotechnology	2 μg/ml (1:100)
Rab11 (47)	mouse IgG2a	Becton Dickinson	25 μg/ml (1:10)
Rac1 (102)	mouse IgG2b	Becton Dickinson	1.25 μg/ml (1:200)
TGN46	rabbit	Thermo Fisher	1.32 μg/ml (1:500)
ZAP70 (discontinued, ref 06-271)	rabbit	Upstate Biotechnology	1:100
Vav1 (M04) (3A11)	mouse IgG2a	Abnova (Interchim)	10 μg/ml (1:100)
Used for activation			
CD3ε (UCHT1)	mouse IgG1	BioLegend Inc.	10 μg/ml
CD28 (28.2)	mouse IgG1	Beckman Coulter	10 μg/ml
Used in flow cytometry			
HIV-1 proteins 55, 39, 33 & 24kD of core antigen (KC57-FITC/FH190-1-1)	mouse IgG1	Beckman Coulter	1:200
Used in western blot			
β-Tubullin (KMX-1)	mouse IgG2b	Millipore	1 μg/ml (1:1000)
Rab11-FIP3	rabbit	www.antibodies-online.com	2.4 μg/ml (1:500)
GAPDH (0411)	mouse IgG1	Santa Cruz Biotechnology	0.1 μg/ml (1:2000)
HIV-1 Nef (6.2) (Lot V9R01009A-004)	mouse IgG1	NIH AIDS Reagent Program	1:500
HIV-1 p24 (AG3.0) (Lot 6 120227)	mouse IgG1	NIH AIDS Reagent Program	1:500
Secondary Antibodies	**Conjugated fluorophore**	**Source**	**Dilution**
Used in immunofluorescence			
Goat anti-Fluorescein/Oregon Green	Alexa Fluor 488	Molecular Probes	10 μg/ml (1:100)
Goat anti-mouse IgG1	Cy3	Jackson ImmunoResearch	15 μg/ml (1:100)
Goat anti-mouse IgG1	Cy5	Jackson ImmunoResearch	7.5 μg/ml (1:200)
Goat anti-mouse IgG2a	Cy3	Jackson ImmunoResearch	7 μg/ml (1:200)
Goat anti-mouseIgG2b	Alexa Fluor 647	Jackson ImmunoResearch	15 μg/ml (1:100)
Goat anti-mouseIgG2b	Cy3	Jackson ImmunoResearch	7.5 μg/ml (1:200)
Goat anti-rabbit	Cy3	Jackson ImmunoResearch	7.5 μg/ml (1:200)
Goat anti-rabbit	FITC	Jackson ImmunoResearch	7.5 μg/ml (1:200)
Used in western blot			
Goat anti-mouse IgG	DyLight800	Thermo Scientific	100 ng/ml (1:10000)
Goat anti-rabbit IgG	DyLight800	Thermo Scientific	62.5 ng/ml (1:8000)

Supplementary Table 1. Primary and secondary antibodies/reagents used for activation, immunofluorescence, flow cytometry and western blot

Gene	Forward	Reverse
B2M	5'-TGACTTTGTCACAGCCCAAGATA-3'	5'-AATGCGGCATCTTCAAACCT-3'
CXCL8	5'-GCCTTCCTGATTTCTGCAGC-3'	5'-TTGGGGTGGAAAGGTTTGGA-3'
FOS	5'-CGAGCGCAGAGCATTGG-3'	5'-CCTTCGGATTCTCCTTTTCTCTT-3'
IL2	5'-ACCTCAACTCCTGCCACAAT-3'	5'-TGAGCATCCTGGTGAGTTTG-3'
IL2RA (CD25)	5'-ATCAGTGCGTCCAGGGATAC-3'	5'-GACGAGGCAGGAAGTCTCAC-3'
IFNG	5'-GAAACGAGATGACTTCGAAAAGCTGAC-3'	5'-CTGCTGGCGACAGTTCAGCCAT-3'
JUN	5'-TGACTGCAAAGATGGAAACG-3'	5'-CAGGGTCATGCTCTGTTTCA-3'
MYC	5'-GAGGCTATTCTGCCCATTTG-3'	5'-CACCGAGTCGTAGTCGAGGT-3'
NFKBIA	5'-GAGCTTTTGGTGTCCTTGGG-3'	5'-CATCAGCCCCACACTTCAAC-3'
TNFAIP3	5'-TAGAAATCCCCGTCCAAGGC-3'	5'-AGCTTCATCCAACTTTGCGG-3'

Supplementary Table 2. Primer sequences